ABSTRACT

HARDER, ABRAM BENNETT. Thermal Conductivity and Permeability of Activated Carbon with Variance in Sample Porosity. (Under the direction of Dr. Richard Gould).

The thermal conductivity of powdered activated carbon was found for two samples of different porosities, and the permeability of a single sample was found. For lower porosities all particles larger than 40μm were sifted out. For the higher porosity an unsifted sample was used.

Thermal conductivity was found to be 0.44 and 0.59 W/m·K for the unsifted and sifted samples, respectively. Pressure drop was measured at various mass and volume flow rates, through the sample and a linear relationship was evident in both. Using pressure drop data the permeability of the unsifted activated carbon was found to be $6.5*10^{-13}$ m^2.

Thermal Conductivity and Permeability of Activated Carbon with Variance in Sample Porosity

by
Abram Bennett Harder

A thesis submitted to the Graduate Faculty of
North Carolina State University
in partial fulfillment of the
requirements for the Degree of
Master of Science

Mechanical Engineering

Raleigh, North Carolina

8/10/2010

APPROVED BY:

_____	_____
Dr. Robert Nagel	Dr. James Leach

_____
Dr. Richard Gould
Chair of Advisory Committee

DEDICATION

This thesis is dedicated to my wife for all the support and encouragement that she gave during this long process.

BIOGRAPHY

The author was born in rural Arkansas, the fourth out of five children. He grew up on a small farm and after graduating from high school he attended Hendrix College, in Conway, Arkansas, where he majored in Physics. The author graduated with distinction and honors before moving to Durham, North Carolina to start graduate school. During his studies at NC State University he took on the role of Graduate Student Team Leader for the EcoCAR Challenge team; where he helped move the team from 16th to 7th place as well as establishing course credit for participation in the competition during his year and a half as team leader.

ACKNOWLEDGMENTS

I would like to thank my advisor, Dr. Gould, for all his help and patience.

TABLE OF CONTENTS

LIST OF TABLES

LIST OF FIGURES

1.0 Introduction

The increasing focus on global warming has intensified the desire to increase fuel efficiency for vehicles using internal combustion engines. New CAFE standards have been set for model years 2012 through 2016 requiring an increase from 29.7 to 34.1 mpg in those four years [1]. It has been estimated that light passenger vehicles and trucks consume 80% of oil imported to the US [2]. One strategy to reduce the amount of energy used is to reduce the accessory loads on the engines of the vehicles. Perhaps the largest accessory load is the air conditioning (AC) compressor, which can account for 12-17% of the energy used during a light passenger vehicle's commute [3]. A source of energy not currently being utilized is the exhaust heat from the engine of the vehicle. This exhaust heat can account for 35% of the energy released from the fuel [3], a potentially large source of energy given its high temperature once the vehicle has warmed up.

There are several different approaches to using the exhaust heat to power an AC system to cool the vehicle; thermoelectric devices, liquid absorption refrigeration, or solid adsorption refrigeration.

Thermoelectric generation is possible but requires a large amount of space to provide the necessary power required to drive an AC compressor. Thatcher et al. [4] developed a prototype thermoelectric generator but were only able to generate approximately 200 W with a system that had a mass of 39.9 kg. In order to generate enough electricity for a vehicle's AC system, 6 kW [3], this thermoelectric generator design would have a mass of 1200 kg.

Boatto et al.[5] looked at using a water-lithium bromide absorption system powered by exhaust heat. They ran into difficulties imposed by the dynamics of being on a moving vehicle. The accelerations and changing orientation of the system led to instabilities in their system. Koehler et al.[6] built a prototype refrigeration system that utilized the ammonia-water pair. Both systems seemed only suited for "long distance driving on flat roads".

In solid adsorption refrigeration systems, the bank of adsorbent must be heated to desorb the working gas, and cooled to re-adsorb it. To have a system that produces continuous cooling

multiple adsorbent banks are alternatively heated and cooled [3]. This also allows for the system to utilize thermal and mass transfer methods to improve the Coefficient of Performance (COP) of the system. Also solid adsorption systems are not as susceptible to the changes in orientation and accelerations as are the liquid absorption systems.

Meunier [7] explored the thermal transfer methods of improving the COP of solid adsorption systems. The uniform temperature adsorber process transfers heat directly from one adsorber bank to the other. This gives only a modest boost to COP as the amount of heat that can be transferred from one adsober to the other is limited as energy is only transferred while they are at different temperatures. An alternative thermal transfer method, the thermal wave process, uses a second loop to transfer heat from the heat source instead of heating the adsorbent banks directly. This second loop also cools the adsorbent banks, allowing the recapture of heat from the adsorbent banks as they are cooled. This process is much more efficient at transferring heat energy from one adsorber to the other.

Another strategy for improved performance is to use mass recovery [8]. For mass recovery the system must have two adsorbers that are out of phase similar to the thermal transfer methods. For mass recovery, the two adsorbers are directly connected via a mass recovery valve. Halfway through the cycle one adsorber is hot and at a high pressure, while the other is cool and at a low pressure. At this point the mass recovery valve is opened and refrigerant travels from the hot adsorber to the cool one until their pressures equalize. Qu et. al. [8] experimentally explored the effects of the mass recovery and found that the mass recovery strategy by itself was only slightly effective, but a coupling with the thermal transfer methods led to the largest improvements in COP.

Wang and Wang [9] looked at the many different approaches to solid adsorption refrigeration. They found that the key to improved COP, once the strategies of thermal and mass transfer have been utilized, was a reduction in cycle time. Two methods are necessary to reduce the cycle time of the system, increases in the flow of mass from the adsorbent bank and increases in the thermal transfer through the adsorbent bank. A common method used to increase thermal transfer is to compact the adsorbent bank. This can greatly increase the heat

transfer through the adsorbent but impedes the mass transfer. Usually the effective thermal conductivity of the adsorber is improved enough to increase the COP in spite of the reduction in mass transfer.

Several authors have evaluated different working pairs for solid adsorption refrigeration. Commonly used pairs include: zeolite-water; silica gel-water; activated carbon-ammonia; activated carbon-methanol [10] [7]. The two pairs that utilize water both have very low vaporization pressures, which require an extra tight vacuum as they are susceptible to air poisoning. Also both systems can freeze in sub-freezing ambient temperatures. Carbon-methanol shows good potential but methanol becomes unstable at temperatures above 393K . Since engine exhaust can average 755K [11], methanol, together with its low working pressure, is unsuitable for this application [12]. For the application of utilizing light vehicle exhaust heat, Lambert et al.[13] has determined that the carbon-ammonia pair is best suited for driving the passenger compartment air conditioning.

Activated carbon comes in many different forms: monolithic; granular; fibre and cloth; powder; and compacted. Tamainot-Telto et al.[14] ran simulations comparing the COP's of systems utilizing the different forms of activated carbon in their adsorber banks. With a driving temperature of 200°C, powdered activated carbon had the highest COP in ice making, as a heat pump, and the air conditioning application. However monolithic carbon had the highest cooling density (MJ/m^3) due to its very high density, 2 to 4 times that of powdered carbon[15][16].

Given the promising cooling density of the monolithic carbon, Critoph and Tamainot-Telto have done work studying adsorption systems with monolithic carbon as the adsober [16][17][18]. Their investigation into monolithic carbon includes its thermophysical properties where they found that this dense carbon had thermal conductivities up to 0.44 W/m·K. When making an air conditioning system for a vehicle, specific cooling power (SCP), cooling energy out per unit mass, is important. Since monolithic carbon is dense, it is made by compressing carbon powder with a binder and pyrolyzation, this leads to a higher SCP. High density also should help increase thermal conductivity making thermal transport

faster in the adsorber bank, thus making shorter cycle times possible [10]. Their earlier prototypes averaged a COP of 0.22 while a newer design utilizing a carbon- aluminum laminate had a COP of about 0.44. This is close to the required COP of 0.6 that was estimated by Lambert [3].

While monolithic carbon is much denser than powdered activated carbon, it can only adsorb half to a third of the ammonia that powdered carbons can [14]. Authors such as Lambert have proposed adsorber banks using powdered adsorbent [3]. Expecting a thermal conductivity lower than monolithic carbon's, Lambert proposed a finned heat exchanger to increase its thermal transport, but to what extent is unknown. It was also assumed that as powdered carbon is less dense than monolithic that the mass transfer would be higher.

The focus of this research is to determine the thermal conductivity of powdered activated carbon and the pressure drop through it and to explore the effects powder porosity on the thermal conductivity. Since enhancements of COP are dependent on increasing thermal or mass transfer to reduce cycle time, a study of powdered carbon is crucial before a properly designed adsorber heat exchanger can be built. While monolithic carbon is very dense and has higher expected thermal conductivity, the expected increase in mass transfer coupled with powdered carbon's higher adsorbance of ammonia could be a promising route in carbon-ammonia systems if the thermal conductivity of powdered carbon is high enough. Porosity will be varied by sifting the powder to separate particles of different sizes. The smaller particles will settle more densely and therefore will have a lower porosity. As the density of the powder bed increases, it is expected that thermal transport should improve. The pressure drop through the sample will be used to find the permeability of the powdered carbon, an important characteristic for design considerations as well.

1.1 Adsorption System Operation

The components of a typical adsorption system are very similar to a vapor compression system, containing a condenser, throttle valve, and evaporator. The compressor is replaced with one or more adsorbers, which provided the pressure gradient to move the working gas

through the system and produce refrigeration. The pressure-temperature cycle for a single adsorber system is shown in Figure 1.1.

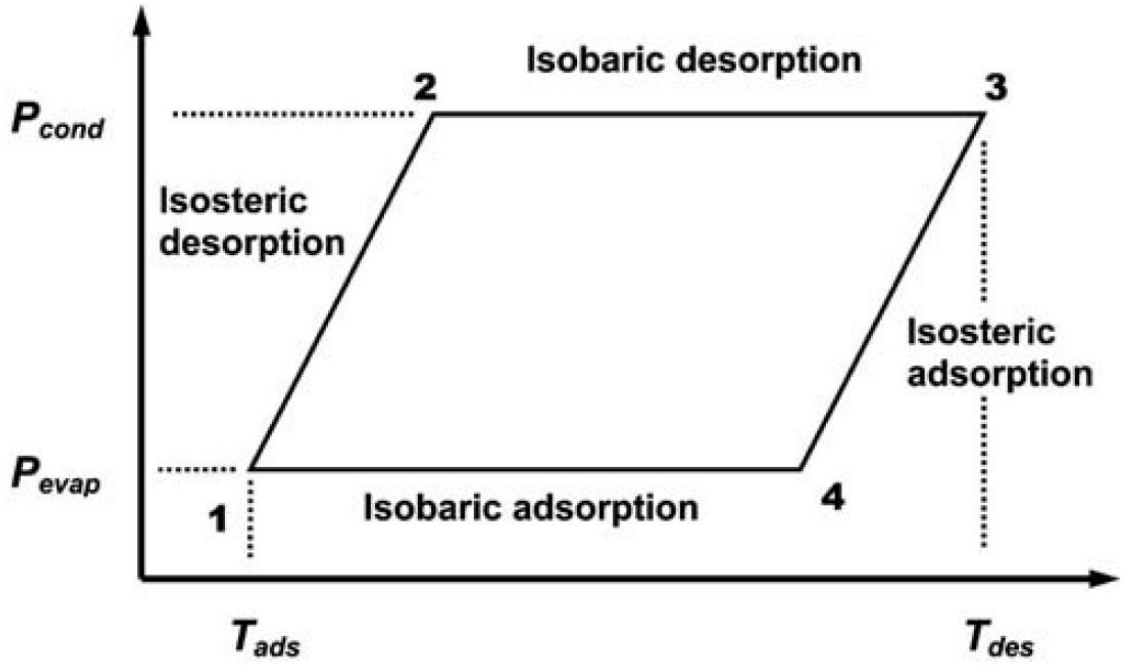

Figure 1.1: Pressure-Temperature graph for single adsorber system[3]

At point 1 the adsorber is at low pressure and temperature and is fully saturated with the working gas. A control valve is used to isolate the adsorber so that desired condensation and evaporation pressures can be reached. The adsorber is heated from points 1 to 2, and the control valve is closed until the desired condensation pressure is reached. While the adsorber is heated working gas desorbs from the adsorbent, increasing the pressure. At point 2 the control valve is opened and working gas moves into the condenser while the adsorber is continued to be heated. At point 3 the adsorbent is fully depleted, and the working gas is all

in the condenser as there is no pressure gradient to draw the working gas through the rest of the system. The control valve is closed again and the adsorber is cooled until the pressure reaches the desired evaporation pressure. At point 4 the control valve is opened and the adsorber is continuing to be cooled as working gas now has a pressure gradient and flows through the rest of the system producing a refrigeration effect. This basic cycle gives broken cooling, and multiple adsorbers must be used for continuous cooling.

Thermal transfer and mass recovery are the two main ways to improve system performance, and systems utilizing these methods are shown in Figures 1.2 and 1.3.

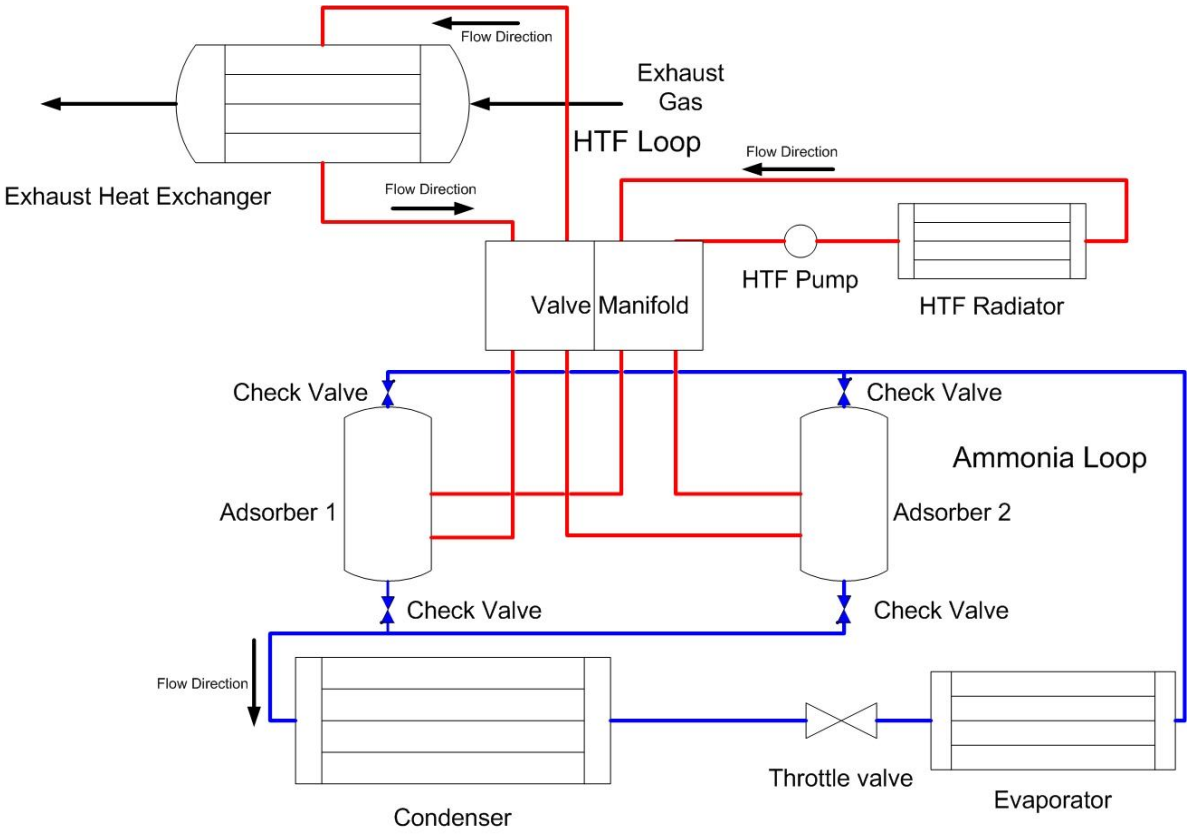

Figure 1.2: Adsorption refrigeration system utilizing thermal transfer method

In Figure 1.2, Heat Transfer Fluid (HTF) lines are shown in Red, while the working gas channels are shown in Blue. A HTF is used instead of directly heating and cooling the adsorbers, which are half a cycle apart. For the explanation of thermal transfer it is assumed that Adsorber 1 is cold and needs to be heated, and Adsorber 2 is hot and needs to be cooled.

- HTF is heated by exhaust before being routed by the valve manifold to Adsorber 1
- After giving energy to Adsorber 1 the HTF is cooled further by ambient air in the HTF radiator
- The HTF is then routed through Adsorber 2, where it gains energy as the Adsorber is cooled
- The HTF is heated further by the exhaust before going back through Adsorber 1

Since COP is designated as $\frac{Q_{out}}{Q_{in}}$ by reusing heat energy from the adsorber being cooled the same output is produced while using less energy from the exhaust, thus improving COP.

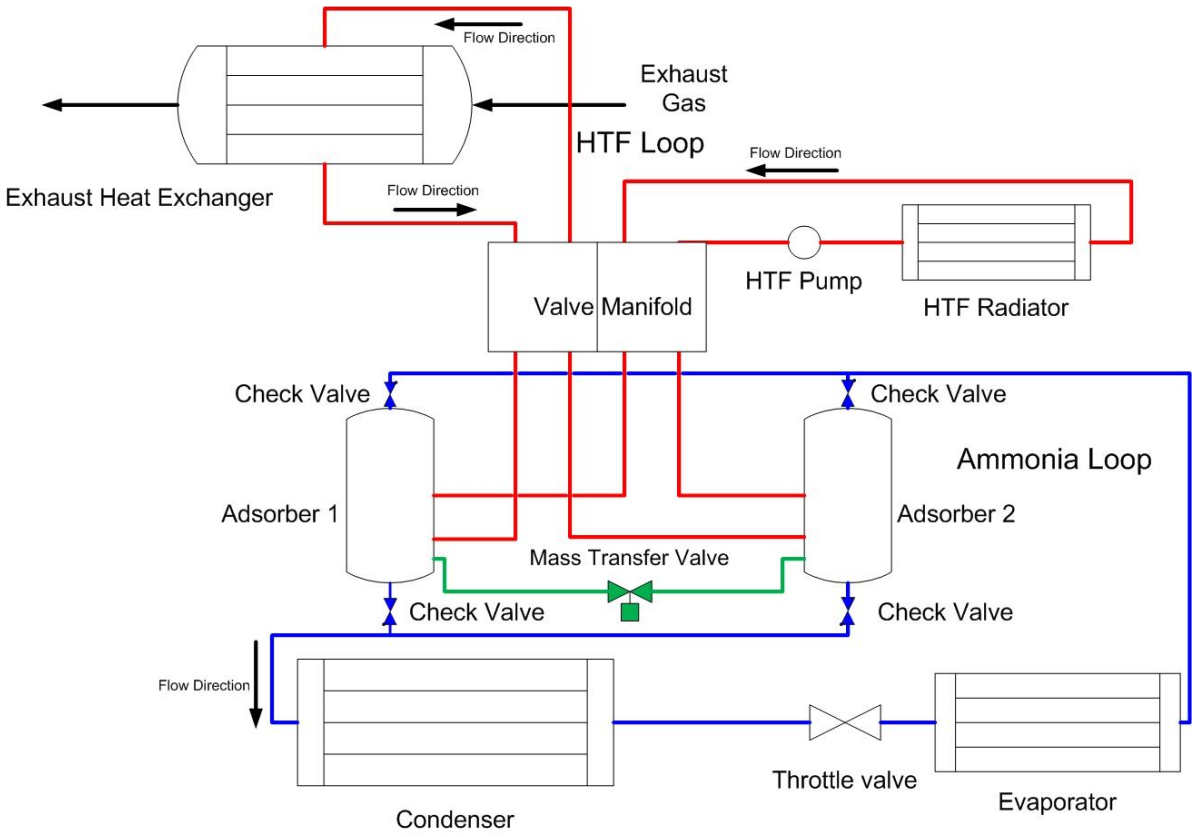

Figure 1.3: Adsorption refrigeration system utilizing mass recovery method

As shown in Figure 1.3, a system that utilizes mass recovery is very similar to one that uses thermal transfer to increase COP. An additional mass recovery line is added, shown in green. For the explanation of mass recovery it is assumed that Adsorber 1 is cold and at low pressure, and Adsorber 2 is hot and at high pressure. This is half way through the cycle and Adsorber 1 is saturated and Adsorber 2 is void of working gas.

- The mass recovery valve opens, while the rest of the check valves are closed, quickly equalizing the two adsorbers' pressures
- Adsorber 1 is heated by the influx of warm working gas, also the increase in pressure induces additional adsorption
- Adsorption is exothermic causing the Adsorber 1 to be further warmed

- Adsorber 2 is cooled by the reduction of pressure, which also causes additional desorption
- The desorption is endothermic further cooling Adsorber 2
- When the pressures are equalized the mass recovery valve is closed and the check valves are reopened.

Mass transfer offers little improvement by itself but when coupled with thermal transfer provided additional improvements to COP over just thermal transfer.

2.0 Methods

2.1 Sifting process

All activated carbon powder used in the experiments was Nuchar SA produced by MeadWestvaco. The carbon powder is made from hardwood sawdust and is chemically activated using a phosphoric acid catalyst. It has an estimated surface area of 1400 to 1800 m^2 per gram of carbon. The activated carbon was screened using a stack of fine stainless steel filter cloths as shown in Figure 2.1.1. The filter cloths were of a twill dutch weave and the particle retention was tested by a screen manufacturer [19].

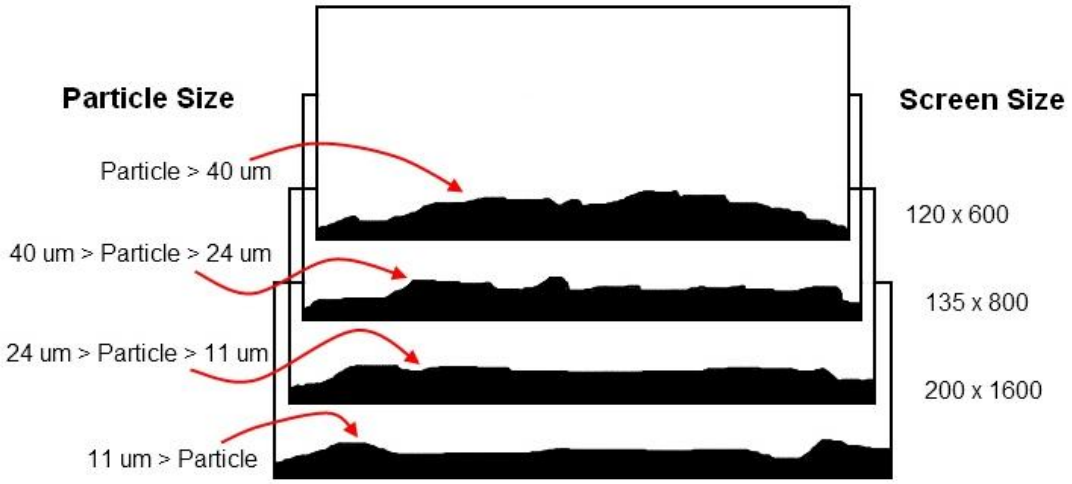

Figure 2.1.1: Sifting apparatus showing particle size and screen mesh density

Raw carbon powder was added to the top and sifted downward due to shaking and agitation. Once the powder had been separated measurements of thermal conductivity and the effects of porosity were studied. It was discovered that the powder exhibits a strong cohesive property and that shaking on a mechanical shaker alone was not enough agitation to promote sifting.

After being on a mechanical shaker for two to three minutes the powder would form a solid block that would not pass through the screen. To restore the powder to a siftable form, small pieces of copper pipe were added to the layers. This allowed, through periodic manual shaking, the powder to remain in a more free flowing state and increased the rate at which powder sifted through the layers.

Initial estimations of particle size were based upon information from the powder manufacture, MeadWestvaco. Their estimate was that 65 to 85 percent of the powder went through a 325 mesh screen and so was less than 45 μm [20]. To properly sift and retain the powder it was determined that a twill dutch weave filter cloth would have the best particle retention. For twill dutch weave mesh the mesh count is warp x weft openings per inch, as the warp wire is a larger diameter than the weft. It was discovered that only a very small percentage of the powder made it through the 135 x 800 mesh screen, with even less going through the 200 x 1600 mesh screen. This could be due to the composition of the powder with a majority of particles being larger than 24μm in diameter, or that it is difficult to force particles that are smaller than 24μm in diameter through a fine screen by gravity only.

Due to the limited amount of carbon that was smaller than 24μm in diameter, and the difficulty in assuring that particles above the 120 x 600 mesh screen were all greater than 40μm in diameter, experiments were conducted with two densities; unsifted powder and powder where the particles were less than 40μm in diameter.

2.2 Determining Porosity

To find the porosity of the samples Eqn. 2.2.1 from Lambert et al. was used [13].

$$Porosity = \left(\forall_{sample} - \frac{M_{sample}}{\rho_{compact}}\right) * \frac{1}{\forall_{sample}} \qquad \text{Eqn. 2.2.1}$$

Where $\forall_{sample}$ is the volume of the sample, M_{sample} is the mass of the sample, $\rho_{compact}$ is the density of activated carbon when it is completely compacted, which Lambert et al.[13] found to be $2210\,\frac{kg}{m^3}$. Volume of the pressure drop apparatus was measured using graduated cylinders. The screen was replaced with plastic to simulate the deflection in the screen which made it difficult to simply measure the height component of the pressure drop apparatus'

volume. The volume measurement was made using 100mL and 25mL graduated cylinders three times and the average taken. For the thermal conductivity experiments, height and diameter measurements were taken using a pair of dial calipers since there was no deflection for this experiment. In both cases the apparatus was weighed before and after the powder was added to find the mass of the powder. With the mass and volume of the powder known it was possible to calculate the porosity. Uncertainty of these measurements is covered in section 3.2.

To determine the powder mass the procedure used was as follows. Powder was first added to the container, and then agitated to promote settling. Additional powder was added to refill the container and the sample was agitated again. This process was repeated until no further settling was visibly detected, at which point the container was weighed to determine the mass of the powder that was added. The uncertainty of the porosity calculations are discussed in section 3.6.

2.3 Thermal Conductivity Measurements

Measurements of the thermal conductivity of the powder were found using a guarded hot plate technique. A schematic of the apparatus is shown in Figure 2.3.1.

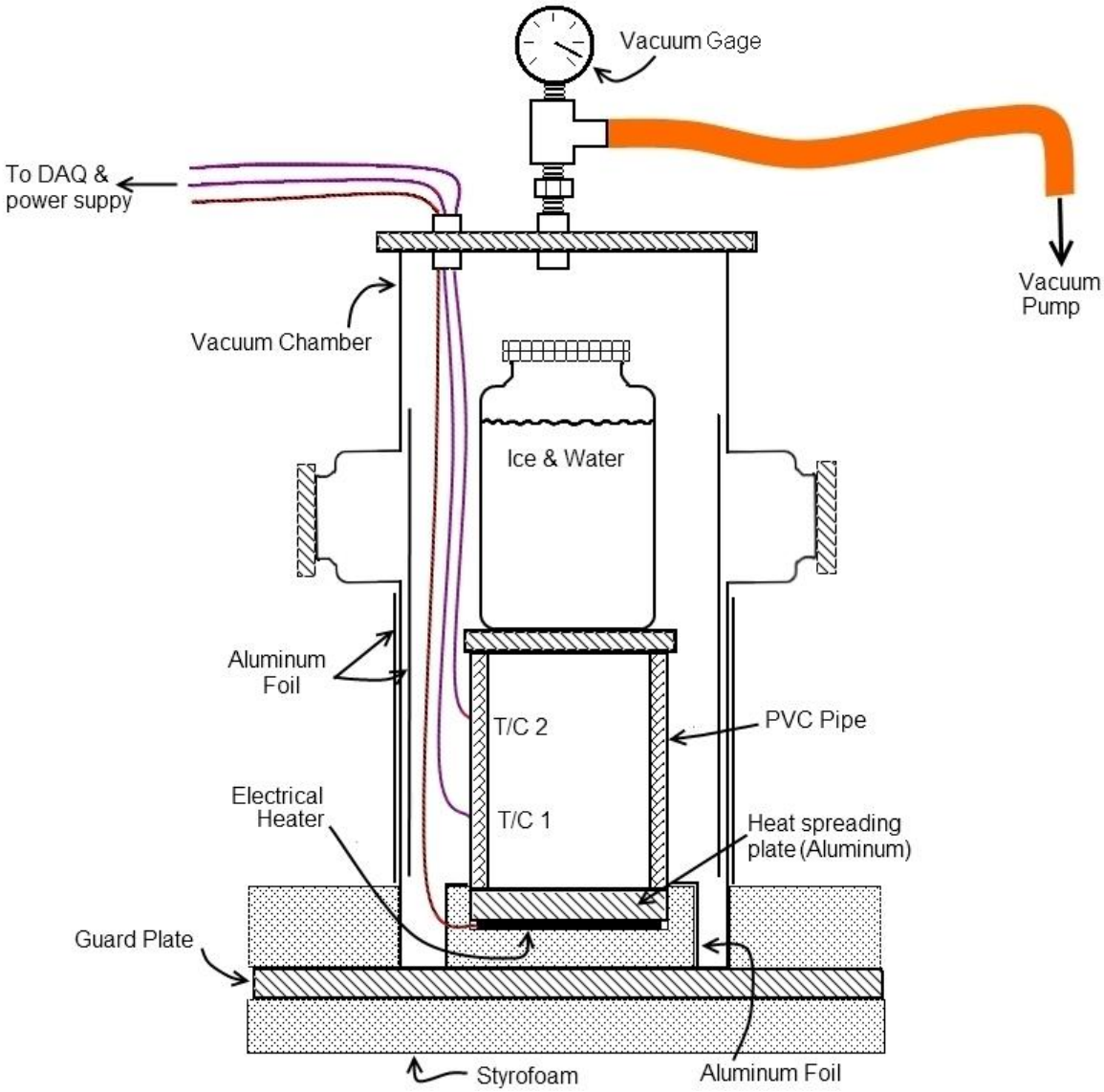

Figure 2.3.1: Thermal Conductivity Apparatus using guarded hot plated method

All thermocouple signals were monitored using an Omega OMB-DAQ-56 analog to digital data acquisition (DAQ) system. This DAQ was interfaced to a computer through a USB cable, allowing for data capture.

The guarded hot plate method consists of a vacuum chamber where the sample, the powdered carbon, is warmed by an electric heater. The sample heater is insulated from the guard plate, which is also warmed to the same temperature at the sample heater; this ensures that all energy from the sample heater passes only through the sample. It is assumed that no energy is being radiated from the sample as the temperatures are kept low and fairly close to the surrounding temperature. No estimation of radiation losses were made, but radiation shields(aluminum foil) were placed between the sample and chamber walls to reduce the exchange between the vacuum chamber and the sample. Any small differences in temperature from the guard plate to the sample heater were measured and the energy flow was calculated using Eqn. 2.3.1

$$q_{in} = q_{htr} + \frac{k_S * A_S}{l_S} \Delta T_{htr} \qquad \text{Eqn. 2.3.1}$$

where q_{in} is the total energy moving through the sample, q_{htr} is the heat energy being produced from the sample heater, k_S is the thermal conductivity of Styrofoam, A_S is the normal area of the Styrofoam, l_S is the thickness of the Styrofoam that separates the sample heater from the guard plate, and ΔT_{htr} is the temperature of the guard plate minus the temperature of the heater. The uncertainty associated with Eqn. 2.3.1 is discussed in section 3.7.

2.3.1 Thermocouples

Two type T thermocouples were used on the guard plate and a third on the sample heater. An average was taken between the two on the guard plate for calculations. A container of ice and water is used as a sink for the energy, to drive conduction in the geometry. Two type T thermocouples were used to measure the temperature of the sample and their separation distance was measured using dial calipers. These thermocouples had an exposed junction and were surrounded by a 0.020" stainless steel sheath. The small diameter and exposed junction gave the thermocouples better response with the fine powder. The thermocouple junction was located at the axis of the 3 inch diameter pipe so as to be in the center of the sample. The

thermocouples were oriented horizontally where the temperature gradient in the radial direction is believed to be small.

Samples of activated carbon powder were contained in three inch diameter foam core PVC pipe. The sample heater was powered by approximately 5.4 VAC and a steady state was reached before measurements of thermal conductivity were made. Uncertainty in the readings from thermocouples is discussed in section 3.3.

2.3.2 Thermocouple Normalization

Due to the inherent error and fluctuations in thermocouple measurements the thermocouples were first normalized so that all thermocouples gave the same temperature reading. With all the thermocouples in equilibrium with the room temperature, a 100 second sample at a rate of one measurement per second was taken. The average value of all five thermocouples was found from the 100 samples. The amount each thermocouple differed from the average was then found. This was used as a calibration offset in the DAQ and another sample of the same size was taken. The average value of all five thermocouples was found from the 100 samples again as well as the amount each thermocouple differed from this average. This second difference was added to the first calibration offset and a new calibration offset was entered into the DAQ. This process was repeated two more times, and the thermocouples were then considered normalized for each sample. While the thermocouples were not calibrated to a known temperature, by normalizing them time averages can be used to find the temperature difference between thermocouples, and effectively remove electrical noise.

2.3.3 Temperature Measurements

The temperature difference was measured once steady state was reached. A sample of 500 seconds at one sample per second was taken and a time average of each reported temperature was used for the final ΔT. The long sample time allowed for confirmation that the temperature differences were steady state.

To find the energy from the sample heater, q_{htr}, Eqn. 2.3.2 was used.

$$q_{htr} = P = \frac{V^2}{R} \qquad \text{Eqn. 2.3.2}$$

Where P is the electrical power input of the heater, V is the voltage difference across the heater, and R is the electrical resistance of the heater which is a function of temperature. The resistance of the heater as a function of temperature was found empirically for both heaters. Resistance was measured every five degrees Centigrade from 110 °C to 20°C. A third order polynomial was then used to fit these measurements. The equation used for the sifted powder's heater is shown in Eqn. 2.3.3.

$$R = -1 * 10^{-7} * T^3 + 2 * 10^{-4} * T^2 + 0.0093 * T + 179.5 \qquad \text{Eqn. 2.3.3}$$

Uncertainty associated with Eqns. 2.3.2 and 2.3.3 is discussed in section 3.7.

2.3.4 Thermal Conductivity of PVC

Due to the low thermal conductivity of the powdered activated carbon, an assessment of the thermal conductivity of the PVC pipe was necessary to accurately calculate the thermal conductivity of the powder. Tseng et al. [21] tested PVC and found thermal conductivities for a range of densities. A sample of the 3 inch foam core PVC pipe was weighed and measured and its density found. Using the values from Tseng et al. an interpolation between the values was made and a thermal conductivity of the PVC calculated. The uncertainty in this thermal conductivity is discussed in section 3.8.

2.3.5 Thermal Conductivity of Activated Carbon

Once the thermal conductivity of the PVC pipe was known it was then possible to compute the thermal conductivity of the powdered carbon from the measured temperature difference. A 1-D heat transfer path was assumed for calculations with the powder and PVC in parallel giving Eqn. 2.3.4.

$$k_{pdr} = \frac{1}{A_{pdr}}\left(\frac{q_{in} * l}{\Delta T_{pdr}} - k_{pvc} A_{pvc}\right) \qquad \text{Eqn. 2.3.4}$$

Where k_{pdr} is the thermal conductivity of the carbon powder, A_{pdr} is the cross sectional area of the carbon powder, l is the distance between the thermocouples, ΔT_{pdr} is the temperature difference between the thermocouples, k_{pvc} is the thermal conductivity of the PVC, and A_{pvc} is the cross sectional area of the PVC. The uncertainty associated with Eqn. 2.3.4 is discussed in section 3.8.

2.4 Pressure drop measurements

Pressure drop measurement were taken with a sample that was 1.04 inches thick in a 4.029 inch inside diameter PVC pipe giving a flow cross sectional area of 0.008225m^2. The apparatus is shown in Figure 2.4.1. The nitrogen enters the 4 inch pipe from the flow meter through a ¼ inch polyethylene tube. A high pressure reservoir allows even flow across the sample. The sample is sandwiched between a set of 325x2300 mesh screens, which has a particle retention capability of 9µm. A coarse common window screen was used to help keep the fine screen from deflecting and bursting under the pressure. The mesh screens are compressed between the lips of the PVC pipe, and a thin layer of vacuum grease together with a thin flat rubber gasket served to seal the joint.

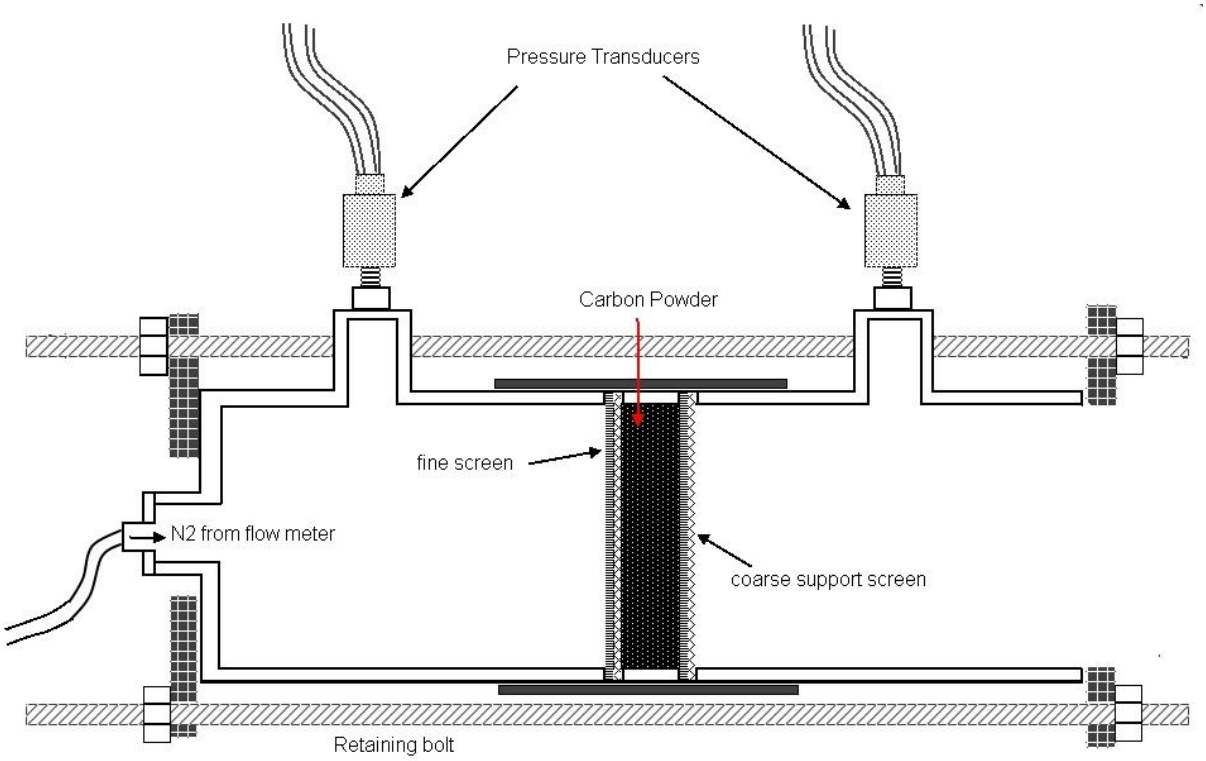

Figure 2.4.1: Pressure drop apparatus.

A schematic of the complete pressure drop setup is shown in Figure 2.4.2.

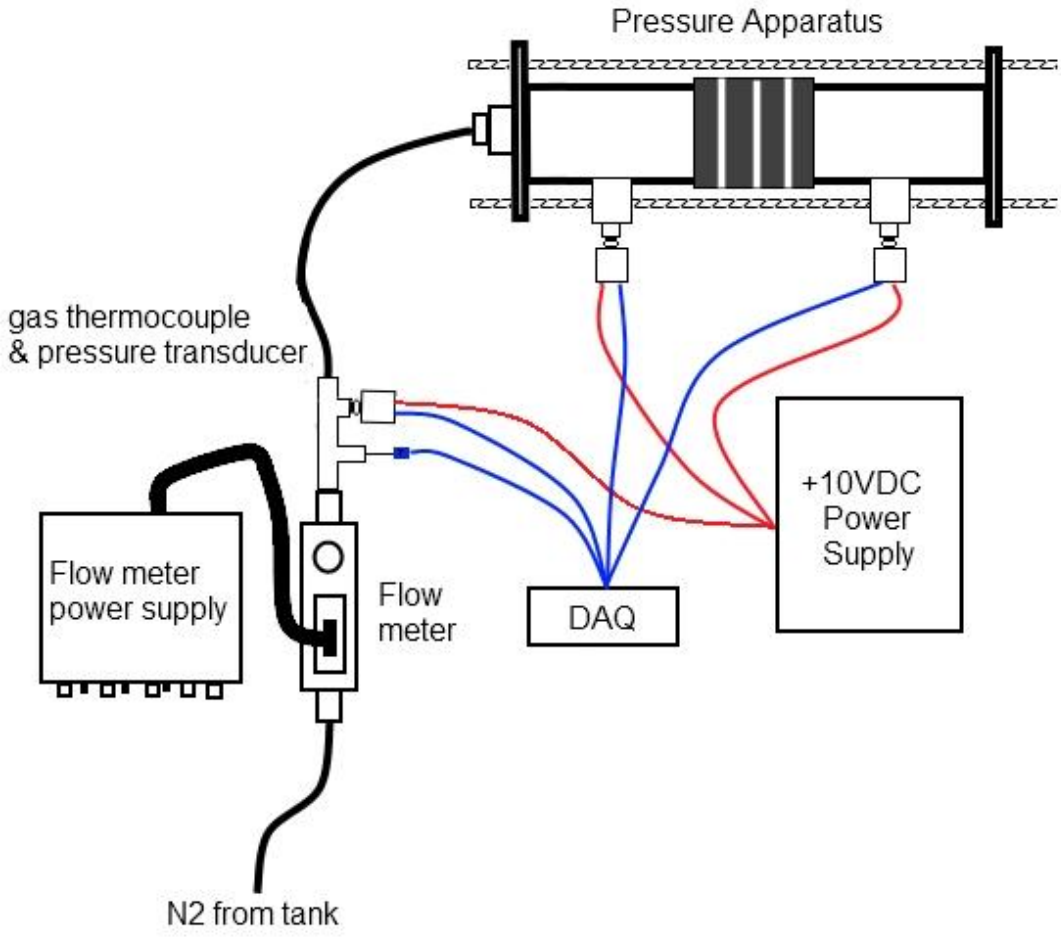

Figure 2.4.2: Delta P system schematic

Nitrogen is routed from the tank through the Teledyne Hastings 203 Series flow meter. The absolute pressure and temperature of the nitrogen is taken immediately after it leaves the meter. This section of pipe is insulated to keep the temperature from being influenced by the ambient temperature. A T type thermocouple was used for the temperature measurement. All pressure transducers were Omega PX01C1-050AV, which require a driving voltage of 10

VDC and have a range from 0 to 50 psi absolute. The signals from the pressure transducers and the thermocouple were monitored by an Omega OMB-DAQ-56 analog to digital DAQ. This DAQ was interfaced to a computer through a USB cable, allowing for data capture. To ensure accuracy in the flow measurements all joints following the flow meter were tested using a gas leak testing fluid to certify that no nitrogen was leaking from the system.

The pressure transducers require an Omega PT1H-10-6P connector. Due to the limited number of connectors that matched the pressure transducers 30 seconds of one measurement per second were taken with an electrical plug on the high pressure side pressure transducer then the plug was switched to the low pressure side and 30 more samples were taken. The pressure transducer that monitored the nitrogen's state immediately after the flow meter was constantly connected. Steady state was reached before any measurements were taken, with both the pressure and temperature of the flow monitored to insure flow conditions were constant. The pressure reading for each respective side was then averaged over the duration for use in calculations. Readings were taken starting at 3L/min increasing by 3 L/min ending with measurements taken at 42L/min, for a total of 14 measurements.

The volume flow meter that was used was originally calibrated for air and so to obtain the mass flow rate of the nitrogen a conversion had to be made. This type of flow meter takes a known part of the flow from a shunt to assure laminar flow through a small tube that is heated. The meter measures the difference in temperature between the two ends of the tube and with a known electrical input it uses calibration fluid properties to calculate the flow using the equation below.

$$\dot{m} = \rho * Q = \frac{q}{C_p * \Delta T}$$

Where ρ is the density of the gas, Q is the volume flow rate, $\dot{m}$ is the mass flow rate, q is the heat energy input, C_p is the heat capacity of the gas, and ΔT is the difference in the temperatures at the two ends of the element.

The pressure transducers give a maximum output of 3mV per volt input. The input voltage was recorded and then multiplied by 0.003 to give maximum output of the pressure

transducer at the transducer's maximum pressure. The scale of the transducers was 0-50psia. Eqn. 2.4.1 was used to find the pressure from the voltage reading of the pressure transducer,

$$P = \frac{50}{V_{max}} V_{out} \qquad \text{Eqn. 2.4.1}$$

where P is the pressure, V_{max} is the maximum output of the pressure transducer, and V_{out} is the measured output voltage of the pressure transducer. Delta P was found by simply subtracting the pressure on the low pressure side from the high side's pressure.

To find Q_{N2} knowing Q_{air}, the volume flow rates of nitrogen and air respectively, as energy input and the temperature difference are the same, so we can take the ratio of the two.

$$\frac{Q_{air}}{Q_{N2}} = \frac{\frac{q}{\rho_{air} c_{p_{air}} \Delta T}}{\frac{q}{\rho_{N2} c_{p_{N2}} \Delta T}}$$

Solving for Q_{N2} we get Eqn. 2.4.2

$$Q_{N2} = Q_{air} \frac{\rho_{air} C_{p_{air}}}{\rho_{N2} C_{p_{N2}}} \qquad \text{Eqn. 2.4.2}$$

where ρ_{air} is the density of air, $c_{p_{air}}$ is the specific heat capacity of air, ρ_{N2} is the density of nitrogen, and $C_{p_{N2}}$ is the specific heat capacity of nitrogen. It was necessary to record the temperature and pressure of the nitrogen as it left the flow meter to later calculate the density of air and nitrogen at the recorded conditions. This was taken in 30 second samples and then time averaged for calculations. To judge whether the ideal gas equation was a viable option for the calculation of the density of the nitrogen and air, the compressibility factor of the gases was analyzed. First the reduced pressure and temperature had to be calculated using Eqn. 2.4.3 And Eqn. 2.4.4

$$P_R = \frac{P}{P_C} \qquad \text{. 2.4.3}$$

$$T_R = \frac{T}{T_C} \qquad \text{Eqn. 2.4.4}$$

where P_R is the reduced pressure, P is the absolute pressure, and P_C is the critical pressure. T_R is the reduced temperature, T is the absolute temperature, and T_C is the critical temperature.

Consulting a generalized compressibility chart [22], and noting that the nitrogen's P_R ranged from approximately 0.03 to 0.06, with a T_R that was approximately 2.354, it was found that nitrogen closely follows the ideal gas law for the range of P_R and T_R seen in this experiment. Wark suggests a ±2% error for nitrogen in this range. For air, the P_R ranged from approximately 0.03 to 0.05 and T_R was approximately 2.234. Air also closely follows the ideal gas law for the range of P_R and T_R seen in this experiment. Since air is comprised of about 80% nitrogen it was assumed to have a ±2% error from the ideal gas law as well.

The density of the nitrogen and air were then found using the ideal gas law, Eqn. 2.4.5.

$$\rho = \frac{P}{RT} \qquad \text{Eqn. 2.4.5}$$

Where ρ is the density, P is the absolute pressure, R is the gas constant, and T is the absolute temperature. Once the densities of nitrogen and air were known, with C_p values at 25°C and 1 atm from Wark [22] it was possible to use Eqn. 2.4.2 to calculate the volume flow rate of the nitrogen, and then calculate the mass flow rate by Eqn. 2.4.6

$$\dot{m}_{N2} = \frac{1}{1000}\rho_{N2}Q_{N2} \qquad \text{Eqn. 2.4.6}$$

where $\dot{m}_{N2}$ is the mass flow rate of the nitrogen in kg per minute. Since flow temperature and pressures were all close to the given values for C_p it was assumed constant throughout this experiment. The uncertainty in flow and pressure calculations are discussed in sections 3.4 and 3.5 respectively.

2.5 Calculating Permeability

Permeability is a measure of a porous material's ability to transmit fluids [23]. A common way of doing this is to use Darcy's law,

$$Q = \frac{KA}{\mu}\frac{\Delta P}{L}$$

where, Q is the volumetric flow, K is the permeability coefficient, A is the cross-sectional area, μ is the viscosity of the fluid, ΔP is the pressure difference across the material, and L is the thickness of the porous material. Darcy's law is only valid for flows where the viscous

forces are much stronger than inertia forces, common in most slow flows. Calculating the Reynolds number (Re) is a common way to compare the two forces,

$$Re = \frac{\nu\rho\delta}{\mu}$$

where υ is the velocity of the flow, ρ is the density, δ is a characteristic diameter in the porous sample (i.e. average pore diameter). Darcy's law is valid where the Re value is less than one. To estimate the Re of the flow the average pore diameter needed to be estimated. It was assumed that the particles were perfect spheres with a conservative diameter of 60μm, as shown in Figure 2.5.1. The space between the four particles is the estimated size of the average pore, $3.14*10^{-5}$m.

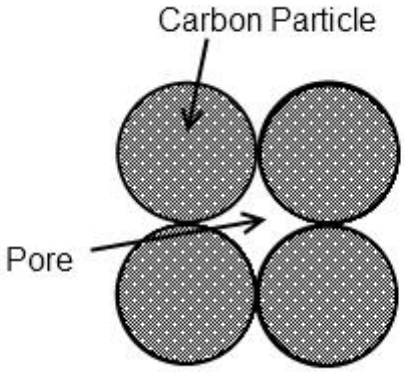

Figure 2.5.1: Assumed pore structure for Re estimation

All calculated Re values were 0.35 or less, meaning that Darcy's law was valid for the flow regimes seen in the pressure drop experiment. Since a gas was being used for the pressure drop experiment the compressibility of the nitrogen must be taken into account with a variation of Darcy's law, Eqn. 2.5.1

$$Q = \frac{KA}{\mu}\frac{P_1^2 - P_2^2}{2PL} \qquad \text{Eqn. 2.5.1}$$

where P_1 is the inlet pressure, P_2 is the outlet pressure, and P is the pressure of the gas where its properties, such as temperature, are measured. To find the permeability of the sample over a range of flow rates Eqn. 2.5.1 is rearranged to get Eqn. 2.5.2,

$$\frac{Q}{A}\frac{\mu}{K} = \frac{\mu}{K}\upsilon = \frac{P_1^2 - P_2^2}{2PL} \qquad \text{Eqn. 2.5.2}$$

where υ is the velocity of the flow. Using Eqn. 2.5.2 it is possible to plot a $\frac{P_1^2 - P_2^2}{2PL}$ vs υ graph. A linear trendline can then be found with the slope being equal to $\frac{\mu}{K}$. It is then possible to solve for the permeability of the sample. The 300K value for μ was used for the nitrogen gas [24]. The uncertainty in the calculation of the permeability of the sample is discussed in section 3.9.

3.0 Uncertainty analysis

Understanding the accuracy of experimental work is crucial when using the measured values for product design or as a reference in a different experiment. Using the method developed by Kline and McClintock [25], the uncertainty in the calculation of the porosity, the thermal conductivity, and the pressure drop can be found and expressed in the form of Eqn. 3.0.1

$$R \pm w_R, (b\ to\ 1) \qquad \text{Eqn. 3.0.1}$$

Where R is the result, w_R is the uncertainty of the result and the range, b to 1, is the odds that the actual result are within the uncertainty range. If the result, R, is a function of several variables such that,

$$R = R(v_1,\ v_2 \ldots v_n)$$

Then to find the uncertainty, w_R, in R, Eqn. 3.0.2 is used

$$w_R = \left[\left(\frac{\partial R}{\partial v_1} w_1\right)^2 + \left(\frac{\partial R}{\partial v_2} w_2\right)^2 + \cdots + \left(\frac{\partial R}{\partial v_n} w_n\right)^2\right]^{1/2} \qquad \text{Eqn. 3.0.2}$$

where w_n is the uncertainty in the variable v_n. Table 3.0.1 is a list of uncertainties of measurement devices used in this experiment. Some uncertainty calculations must be done for each measurement as they are based upon a percentage of the reading or when the uncertainty is computed using Eqn. 3.0.2 measurement terms are left in the equation that must be evaluated.

Table 3.0.1: Measurement Uncertainties

Measurement Type	Uncertainty	Reference
T type thermocouple	±0.5°C or 0.4% whichever is greater	[26]
DAQ T type thermocouple error	±0.4°C and ±0.5°C cold junction compensation	[27]
DAQ Voltage reading error	0.01% of reading + 0.002% of range (selected range = ±0.0310)	[27]
Pressure transducer error	output ±0.25% & linearity ±0.05%	[28]
Voltmeter error	±0.04% + 2 digits for DC; ±3% + 200 digits for AC	[29]
Ohmmeter error	±0.07% + 2 digits +0.02Ω	[29]
Scale mass error	±0.05g	[30]
Graduated cylinder (100 mL)	±1.0 mL	[31]
Graduated cylinder (25mL)	±0.5 mL	[31]
Flow meter volume flow rate error	±1% full scale (1 L/min)	[32]
Dial calipers	±0.0005 inches	[33]

3.1 Uncertainty in liquid volume measurement

Each measurement of the volume required using the 100 mL graduated cylinder twice and the 25mL graduate cylinder three times, as shown below.

$$\forall_{g,1} = \forall_{100,1} + \forall_{100,2} + \forall_{25,1} + \forall_{25,2} + \forall_{25,3}$$

Where $\forall_{g,1}$ is the first of three volume measurements of the pressure apparatus, $\forall_{100,n}$ is the first or second volume measurement made by a 100mL graduated cylinder, and $\forall_{25,n}$ is a

volume measurement made by a 25mL graduated cylinder. Therefore the uncertainty in one measurement of the volume of the pressure apparatus was,

$$w_{g,1} = \left[\left(\frac{d\forall_{g,1}}{d\forall_{100,1}} w_{100}\right)^2 + \left(\frac{d\forall_{g,1}}{d\forall_{100,2}} w_{100}\right)^2 + \left(\frac{d\forall_{g,1}}{d\forall_{25,1}} w_{25}\right)^2 + \left(\frac{d\forall_{g,1}}{d\forall_{25,2}} w_{25}\right)^2 + \left(\frac{d\forall_{g,1}}{d\forall_{25,3}} w_{25}\right)^2\right]^{1/2}$$

$$w_{g,1} = [2 * {w_{100}}^2 + 3 * {w_{25}}^2]^{1/2} = 1.65831mL \qquad \text{Eqn. 3.1.1}$$

Where $w_{g,1}$ is the uncertainty in the first volume measurement of the pressure apparatus, w_{100} is the uncertainty in a measurement made by a 100mL graduated cylinder, and w_{25} is the uncertainty in a measurement made by a 25mL graduated cylinder. Since three measurements were made and the average taken the final volume, $\forall_g$ is expressed as,

$$\forall_g = \frac{1}{3}(\forall_{g,1} + \forall_{g,2} + \forall_{g,3})$$

Also the uncertainty of the three volume measurements are equal so $w_{g,1} = w_{g,2} = w_{g,3}$, giving as the total uncertainty, w_g, in Eqn. 3.1.2

$$w_g = \left[\left(\frac{d\forall_g}{d\forall_{g,1}} w_{g,1}\right)^2 + \left(\frac{d\forall_g}{d\forall_{g,2}} w_{g,1}\right)^2 + \left(\frac{d\forall_g}{d\forall_{g,3}} w_{g,1}\right)^2\right]^{1/2}$$

$$= \left[\left(\frac{1}{3} w_{g,1}\right)^2 + \left(\frac{1}{3} w_{g,1}\right)^2 + \left(\frac{1}{3} w_{g,1}\right)^2\right]^{1/2} = \left[\frac{3}{9} w_{g,1}^2\right]^{1/2}$$

$$w_g = \sqrt{\frac{1}{3}} w_{g,1} = 0.957247mL \qquad \text{Eqn. 3.1.2}$$

The uncertainty of the volume found by the graduated cylinders is dominated by the large uncertainty of the 100ml cylinder, using a more precise volume measuring tool, such as the 25mL cylinder, would have reduced the uncertainty.

3.2 Uncertainty in volume and area measurements using calipers

Calipers where used to measure the height and diameter of a cylinder for the thermal conductivity experiments, with the equation below used to calculate the volume,

$$\forall = h * \frac{\pi}{4} * D^2$$

where h is the height of the cylinder and D is the diameter. The uncertainty in this calculation is calculated using the Kline & McClintock(1953) method.

$$w_\forall = \left[\left(\frac{\pi}{4} D^2 w_c\right)^2 + \left(h\frac{\pi}{2} D\, w_c\right)^2\right]^{1/2} = \left[\left(\frac{\pi^2}{16} D^4 {w_c}^2\right) + \left(h^2 \frac{\pi^2}{4} D^2\, {w_c}^2\right)\right]^{1/2}$$

where $w_\forall$ is the uncertainty in a volume measurement taken by calipers, and w_c is the uncertainty in the measurement by a dial caliper. A better way is to divide $w_\forall$ by $\forall$, giving Eqn. 3.2.1

$$\frac{w_\forall}{\forall} = \left(\frac{{w_c}^2}{h^2} + \frac{4w_c^2}{D^2}\right)^{1/2} \qquad \text{Eqn. 3.2.1}$$

Similarly for cross sectional areas such as A_S or A_{pdr} Eqn. 3.2.2 was used.

$$\frac{w_A}{A} = \frac{2w_c}{D} \qquad \text{Eqn. 3.2.2}$$

Where w_A is the uncertainty in the cross sectional area as measured by a pair of dial calipers, and A is the area. For things like A_{pvc} which is a ring Eqn. 3.2.3 was used.

$$w_{ring} = \frac{\pi}{2} w_c (D_{out}^2 + D_{in}^2)^{1/2} \qquad \text{Eqn. 3.2.3}$$

Where w_{ring} is the uncertainty in the cross sectional area of a PVC pipe. The uncertainty in the volume of the material of a PVC pipe is given in Eqn. 3.2.4.

$$w_{\forall_{pvc}} = \frac{\pi}{4}\{[w_c(D_{out}^2 - D_{in}^2)]^2 + (2hD_{out}w_c)^2 + (2hD_{in}w_c)^2\}^{1/2} \qquad \text{Eqn. 3.2.4}$$

All uncertainties are dominated by the uncertainty in the measurement by the dial calipers.

3.3 Uncertainty in Temperature

There are inherent uncertainties in making a temperature measurement with a single thermocouple, both in the device itself and in the DAQ system. For the uncertainty in a single temperature reading, w_{TC}, it is necessary to analyze the three uncertainties in the measurement: the error in the device itself; erroneous cold junction compensation in the DAQ; and uncertainty in calculating the temperature from the output voltage from the thermocouple by the DAQ. While not stated in the DAQ user's manual, it is assumed that a

7^{th} order polynomial is used to interpret the output voltage of the thermocouple with an uncertainty of ±0.5°C, with the coefficients, a_n, given by Holman [34] is given in Eqn. 3.3.1

$$T = a_0 + a_1 V + a_2 V^2 + \cdots + a_7 V^7 \qquad \text{Eqn. 3.3.1}$$

where V is the output voltage of thermocouple, T is the temperature, and a_n is coefficient. However, uncertainties in temperature measurements from thermocouples are given in terms of end temperature not output voltage. The value for w_{TC} is shown in Eqn. 3.3.2, and is simply the three uncertainties in the temperature added together.

$$w_{TC} = 0.5 + 0.4 + 0.5 = 1.40°\text{C} \qquad \text{Eqn. 3.3.2}$$

Because these temperature uncertainties are believed to be random, 500 samples were taken for the thermal conductivity experiments and 30 for the pressure drop. The uncertainty for a temperature measurement is then expressed by Eqn. 3.3.3 for a 95% confidence interval on a large number of measurements [34].

$$w_T = 1.96 * \frac{\sigma}{\sqrt{n}} \qquad \text{Eqn. 3.3.3}$$

Where w_T is the uncertainty in a temperature measurement, n is the number of samples taken, and σ is the standard deviation of the measurements from the thermocouple. w_T was calculated for temperature measurements of the sample heater, the two sample temperatures, and the two guard plate temperatures for the unsifted and sifted powder samples. For temperature difference is was necessary to use the Kline & McClintock[25] method. The uncertainty in ΔT_{pdr} and ΔT_{htr} are expressed in equations Eqn. 3.3.4 and Eqn. 3.3.5, respectively.

$$w_{pdr} = [(w_{T,1})^2 + (w_{T,2})^2]^{1/2} \qquad \text{Eqn. 3.3.4}$$

where w_{pdr} is the uncertainty in ΔT_{pdr}. For ΔT_{htr} the temperature of the guard plate is an average between two thermocouples and so the uncertainty requires an extra step.

$$w_{GP} = \left[\left(\frac{1}{2} w_{T,1}\right)^2 + \left(\frac{1}{2} w_{T,2}\right)^2\right]^{1/2}$$

where w_{GP} is the uncertainty in the temperature of the guard plate, and $w_{T,n}$ is the uncertainty of one of the two thermocouples on the guard plate.

$$w_{htr} = [(w_{GP})^2 + (w_T)^2]^{1/2} \quad \text{Eqn. 3.3.5}$$

where w_{htr} is the uncertainty in ΔT_{htr}. The large uncertainty in a single measurement from a thermocouple requires the average of a large number of temperature measurements to reduce the uncertainty.

3.4 Uncertainty in Pressure

When finding uncertainty in Eqn. 2.4.1 three variables must be considered: V_{max}; V_{out}; and the linearity of the pressure transducer. To calculate the uncertainty in V_{max} by starting with the equation below,

$$V_{max} = V_{excite} * \frac{mV}{V}$$

where V_{excite} is the excitation voltage applied to the pressure transducer, and $\frac{mV}{V}$ is the millivolt out per volt in ratio. The uncertainty for V_{max} is expressed in Eqn. 3.4.1,

$$w_{max} = \left[\left(w_{vmeter} * \frac{mV}{V}\right)^2 + \left(V_{excite} * w_{mV/V}\right)^2\right]^{1/2} \quad \text{Eqn. 3.4.1}$$

where w_{max} is the uncertainty in $V_{max.}$ While V_{out} is an average of 30 samples to remove electrical noise, Eqn. 3.4.2 was used for its uncertainty,

$$w_{out} = 0.0025 * V_{out} \quad \text{Eqn. 3.4.2}$$

where w_{out} is the uncertainty for V_{out}, the output from the pressure transducer. The uncertainty in the linearity is given by the manufacture of the pressure transducer. Thus for the uncertainty in the pressure we get,

$$w_P = \left[\left(\frac{V_{out}}{V_{max}} w_{linear}\right)^2 + \left(\frac{V_{out}}{V_{max}^2} * linear * w_{\max}\right)^2 + \left(\frac{linear}{V_{max}} w_{out}\right)^2\right]^{1/2}$$

Where w_P is the uncertainty for the pressure and w_{linear} is the uncertainty in the linearity of the pressure transducer. For a more useful equation we can divide by Eqn. 2.4.1 to get Eqn. 3.4.3.

$$\frac{w_P}{P} = \left[\frac{w_{linear}^2}{linear^2} + \frac{w_{max}^2}{V_{max}^2} + \frac{w_{out}^2}{V_{out}^2}\right]^{1/2} \quad \text{Eqn. 3.4.3}$$

Where *linear* is the linearity, here 0 to 50 for the pressure transducers used. To find the uncertainty in the change of pressure we get Eqn. 3.4.4

$$w_{\Delta P} = \left[\left(w_{P,high}\right)^2 + \left(w_{P,low}\right)^2\right]^{1/2} \quad \text{Eqn. 3.4.4}$$

The uncertainty in the pressure measurements is dominated by the uncertainty in the output of the pressure transducer, w_o, and the uncertainty in the linearity of the output, w_{linear}. The uncertainty, w_{max}, was negligible.

3.5 Uncertainty in Flow Measurement

The uncertainty for Q_{N2} in Eqn. 2.4.2 is given below, however a much more useful form of the equation is given as Eqn. 3.5.1

$$w_{N2} = \frac{c_{P_{air}}}{c_{P_{N2}}}\left[\left(\frac{\rho_{air}}{\rho_{N2}} w_{Q_{air}}\right)^2 + \left(\frac{Q_{air}}{\rho_{N2}} w_{\rho_{air}}\right)^2 + \left(\frac{Q_{air}\rho_{air}}{\rho_{N2}^2} w_{\rho_{N2}}\right)^2\right]^{1/2}$$

$$\frac{W_{N2}}{Q_{N2}} = \left[\frac{w_{Q_{air}}^2}{Q_{air}^2} + \frac{w_{\rho_{air}}^2}{\rho_{air}^2} + \frac{w_{\rho_{N2}}^2}{\rho_{N2}^2}\right]^{1/2} \quad \text{Eqn. 3.5.1}$$

Where w_{N2} is the uncertainty in the calculated volume flow of nitrogen through the system, $w_{Q_{air}}$is the uncertainty in the volume flow measurement from the meter, and $w_{\rho_{air}} = w_{\rho_{N2}} =$ 2% [22]and is the uncertainty in the density of the air and nitrogen. To get the uncertainty for the mass flow rate of the nitrogen we use Eqn. 3.5.1 and apply the Kline McClintock method to Eqn. 2.4.6 to get Eqn. 3.5.2.

$$w_{\dot{m}} = \frac{1}{1000}\left[(Q_{N2} w_\rho)^2 + (\rho_{N2} w_{N2})^2\right]^{1/2} \quad \text{Eqn. 3.5.2}$$

Where w_m is the uncertainty in the mass flow rate. The uncertainty in the volume and mass flow rates of nitrogen is dominated by the uncertainty in the volume flow rate from the Hastings series 203 flow meter. The uncertainty in the density of air and nitrogen are almost negligible.

3.6 Uncertainty in Porosity calculation

When finding the uncertainty in the calculation of the porosity it is easier to do so if Eqn. 2.2.1 is rewritten as:

$$Porosity = 1 - \frac{M_{sample}}{\forall_{sample} * \rho_{compressed}}$$

The uncertainty in $\rho_{compact}$ is not stated by Lambert et al. [13]. To estimate the uncertainty Eqn. 3.6.1 is used.

$$w_{\rho_{compact}} = \left[\left(\frac{w_M}{\forall_{sample}}\right)^2 + \left(\frac{M_{sample}}{\forall_{sample}^2} w_{\forall_{sample}}\right)^2\right]^{1/2} \qquad \text{Eqn. 3.6.1}$$

For the calculation of Eqn. 3.6.1 the mass of the sample was taken to be 2.210kg and the volume was 1/1000 of cubic meter. The uncertainties of the mass and volume are the same as those in Table 3.0.1 or previously calculated for a volume measurement using calipers.

Then the uncertainty for porosity is found from Eqn. 3.6.2

$$w_{Porosity} = \left[\left(\frac{w_M}{\forall_{sample} * \rho_{compact}}\right)^2 + \left(\frac{w_{\forall_{sample}} M_{sample}}{\forall_{sample}^2 * \rho_{compact}}\right)^2 + \left(\frac{w_{\rho_{compact}} M_{sample}}{\forall_{sample} * \rho_{compact}^2}\right)^2\right]^{1/2} \qquad \text{Eqn. 3.6.2}$$

For Eqn. 3.6.1 neither uncertainty term dominates, while in Eqn. 3.6.2 the uncertainty in $\rho_{compact}$ is negligible.

3.7 Uncertainty in Energy Input Calculations

Before it is possible to calculate the uncertainty in q_{in} from Eqn. 2.3.1 the uncertainties of q_{htr} and the resistance of the heater must be calculated. The resistance of the heater is modeled well by a third order polynomial with temperature as the variable, using the resistance equation for the unsifted powder gives Eqn. 3.7.1.

$$w_R = \{[(6 * 10^{-7}T^2 - 6 * 10^{-5}T + 0.031)w_{TC}]^2\}^{1/2} \qquad \text{Eqn. 3.7.1}$$

Now with w_R known it is possible to calculate the uncertainty of q_{htr}, Eqn. 2.3.2, as done in Eqn. 3.7.2

$$w_{q_{htr}} = \left[\left(\frac{2V}{R} w_{vmeter}\right)^2 + \left(\frac{V^2}{R^2} w_R\right)^2\right]^{1/2} \qquad \text{Eqn. 3.7.2}$$

Finally, the uncertainty in the energy input, Eqn. 2.3.1, into the thermal conductivity experiment can be found with Eqn. 3.7.3

$$w_{q_{in}} = \left[(w_{q_{htr}})^2 + (\tfrac{A_s}{l_s}\Delta T_{htr} w_{k_s})^2 + (\tfrac{k_s}{l_s}\Delta T_{htr} w_A)^2 + (\tfrac{A_s k_s}{l_s^2}\Delta T_{htr} w_c)^2 + (\tfrac{k_s A_s}{l_s} w_{htr})^2\right]^{1/2} \qquad \text{Eqn. 3.7.3}$$

Budaiwi et al. [35] gave the uncertainty for k_s as ±3%. In Eqn. 3.7.2 w_R dominates and w_{vmeter} is negligible. While in Eqn. 3.7.3 w_A is completely negligible and w_c could be neglected with only a small effect.

3.8 Uncertainty in thermal conductivity calculations

Before calculating the uncertainty in the thermal conductivity of the carbon powder, it is necessary to calculate the uncertainty in the assumed value of thermal conductivity of the PVC. While Tseng et al.[21] does not state the uncertainty in the range of thermal conductivities that is recorded, Tseng et al. used a guarded hot plate method and so the uncertainty can be calculated for Eqn. 3.8.1, as this would be the equation used to find the thermal conductivity of the PVC using the guarded hot plate method.

$$k_{pvc,thry} = \frac{q_{in} l}{\Delta T A_{pvc}} \qquad \text{Eqn. 3.8.1}$$

Where $k_{pvc,thry}$ is the theoretical thermal conductivity of PVC pipe using the guarded hot plate method. The uncertainty of $k_{pvc,thry}$ is estimated in Eqn. 3.8.2

$$\frac{w_{k_{pvc,thry}}}{k_{pvc,thry}} = \left[\frac{w_{q_{in}}^2}{q_{in}^2} + \frac{w_c^2}{l^2} + \frac{w_{pdr}^2}{\Delta T^2} + \frac{w_{ring}^2}{A_{pvc}^2}\right]^{1/2} \qquad \text{Eqn. 3.8.2}$$

To evaluate Eqn. 3.8.2 values need to be estimated for q_{in}, l, ΔT, and A_{pvc} since these are not specified by Tseng et al.[21] The same value for A_{pvc} was chosen as was used in the thermal experiment, and q_{in} was assumed to be the same as for the thermal experiment on the unsifted powder. l was assumed to be 0.05m giving a ΔT of 24.61°C. The $w_{q_{in}}^2$ and w_{pdr}^2 values were taken from the unsifted powder uncertainty estimations. The uncertainty w_c could be neglected from Eqn. 3.82. To calculate an assumed PVC thermal conductivity, a liner interpolation of the range stated by Tseng et al. was used. The formula used was Eqn. 3.8.3,

$$k_{pvc} = \frac{5-3.5}{1.58-1.3} * \frac{4.184}{100} SG_{pvc} - 3.46426 \qquad \text{Eqn. 3.8.3}$$

where SG_{pvc} is the specific gravity of the 3 inch foam core PVC pipe. The density of the PVC was found by measuring a sample with dial calipers and finding its mass with a scale. The uncertainty in ρ_{pvc} is given in Eqn. 3.8.4

$$w_{\rho_{pvc}} = \left[\left(\frac{w_M}{\forall_{pvc}}\right)^2 + \left(\frac{M_{pvc} w_{\forall_{pvc}}}{\forall_{pvc}^2}\right)^2\right]^{1/2} \quad \text{Eqn. 3.8.4}$$

In Eqn.3.8.4 the uncertainty in the mass of the PVC dominates. Now it is possible to compute the uncertainty on the assumed PVC thermal conductivity, as shown in Eqn. 3.8.5

$$w_{k_{pvc}} = \frac{4.184}{100}\left[2\left(\frac{w_{k_{pvc,thry}}}{0.28} SG_{pvc}\right)^2 + 2\left(\frac{1.5}{0.0784} SG_{pvc} w_{\rho_{pvc}}\right)^2 + \left(\frac{1.5}{0.28} w_{\rho_{pvc}}\right)^2\right]^{1/2} \quad \text{Eqn. 3.8.5}$$

Eqn. 3.8.5 is dominated by $w_{\rho pvc}$. Finally, it is possible to find the uncertainty in the thermal conductivity of the carbon powder, from Eqn. 2.3.4, this is shown in Eqn. 3.8.6

$$w_{k_{pdr}} = \left\{\left[\frac{w_A}{A_{pdr}^2}\left(\frac{q_{in} l}{\Delta T_{pdr}} - k_{pvc} A_{pvc}\right)\right]^2 + \left(\frac{w_{q_{in}} l}{A_{pdr}\Delta T_{pdr}}\right)^2 + \left(\frac{q_{in} w_c}{A_{pdr}\Delta T_{pdr}}\right)^2 + \left(\frac{q_{in} l}{A_{pdr}\Delta T_{pdr}^2} w_{pdr}\right)^2 + \left(\frac{w_{k_{pvc}} A_{pvc}}{A_{pdr}}\right)^2 + \left(\frac{k_{pvc} w_{ring}}{A_{pdr}}\right)^2\right\}^{1/2} \quad \text{Eqn. 3.8.6}$$

Eqn. 3.8.6 is not dominated by any particular uncertainty but w_c and w_{ring} are negligible.

3.9 Uncertainty in Permeability Calculation

There are two parts to the uncertainty in the calculation of the permeability of the carbon sample. Since a graph of $\frac{P_1^2 - P_2^2}{2PL}$ vs υ was used to find the permeability, K, then the uncertainty in the values of $\frac{P_1^2 - P_2^2}{2PL}$ and υ must be found. The uncertainty for $\frac{P_1^2 - P_2^2}{2PL}$ is shown in Eqn. 3.9.1

$$w_{K,P} = \left[\left(\frac{P_1 w_{P_1}}{P_{gas} L}\right)^2 + \left(\frac{P_2 w_{P_2}}{P_{gas} L}\right)^2 + \left(\frac{P_1^2 - P_2^2}{P_{gas}^2 L} w_{P_{gas}}\right)^2 + \left(\frac{P_1^2 - P_2^2}{P_{gas} L^2} w_c\right)^2\right]^{1/2} \quad \text{Eqn. 3.9.1}$$

where $w_{K,P}$ is the uncertainty in $\frac{P_1^2 - P_2^2}{2PL}$, P_1 is the pressure before the carbon sample, P_2 is the pressure down flow from the sample, P_{gas} is the pressure where nitrogen properties, such as temperature, are measured, and the w_P's are the uncertainty in the associated pressure. Eqn. 3.9.1 is dominated by the uncertainties in the high and low pressures. The uncertainty in the flow velocity is shown in Eqn. 3.9.2,

$$w_\nu = \left[\left(\frac{w_{Q_{N2}}}{A}\right)^2 + \left(\frac{Q_{N2} w_A}{A^2}\right)^2\right]^{1/2} \quad \text{Eqn. 3.9.2}$$

Eqn. 3.9.2 is dominated by the uncertainty in the volume flow of nitrogen.

3.10 Summary of Uncertainty

Table 3.10.1 contains a summary of the calculated uncertainties. Uncertainties for pressure and permeability are not included due to the large number of data points, but error bars are included on figures shown in Section 4.

Table 3.10.1 Summary of Uncertainties

Variable	Uncertainty of Variable		Uncertainty	Percent of Variable
ΔT_{pdr}(K)	w_{pdr}	unsifted	0.0108	0.36
		Sifted	0.0056	0.10
q_{in} (W)	$w_{q_{in}}$	unsifted	0.0041	0.32
		Sifted	0.0005	0.12
k_{pdr} (W/m·K)	$w_{k_{pdr}}$	unsifted	0.0300	6.9
		Sifted	0.0406	6.8
Porosity (Thermal)	$w_{Porosity}$	unsifted	5.971E-5	7.02E-3
		Sifted	0.0001	0.02
Porosity (Pressure)	$w_{Porosity}$	unsifted	0.0001	0.02
		Sifted	0.0002	0.02
k_{pvc} (W/m·K)	$w_{k_{pvc}}$		0.0048	3.0

4.0 Results

4.1 Thermal Conductivity Results

Results for the thermal conductivity of powdered activated carbon were found for unsifted and sifted samples. The porosity and density of these samples was found as well. The resistance to flow through the powdered carbon was measured by a pressure drop through a sample of the unsifted powder. The pressure drop was recorded for various volume and mass flow rates. Thermal conductivity and density measurements are summarized in Table 4.1.1.

Table 4.1.1: Summary of Thermal Conductivity Measurements

	Density (kg/m^3)	Porosity	Thermal Conductivity (W/m·K)
Unsifted	329.5 ±0.13 (0.04%)	0.851 ±5.9E-5 (7.02E-3%)	0.43 ±0.03 (6.9%)
Sifted	542.6 ±0.27 (0.05%)	0.754 ±1.25E-4 (0.02%)	0.59 ±0.04 (6.8%)

Table 4.1.2 shows the changes in density, porosity, and thermal conductivity due to sifting.

Table 4.1.2: Changes in Powder Properties Due to Sifting (Sifted vs. Unsifted)

% density increase	% decrease in Porosity	% increase in Thermal Conductivity
64.643	11.330	35.882

4.2 Pressure Drop and Permeability Results

Results for the pressure drop experiment are summarized in Figures 4.2.1 and 4.2.2, showing pressure drop versus volume flow and mass flow rates, respectively. Error bars are included to show the uncertainty associated with each measurement.

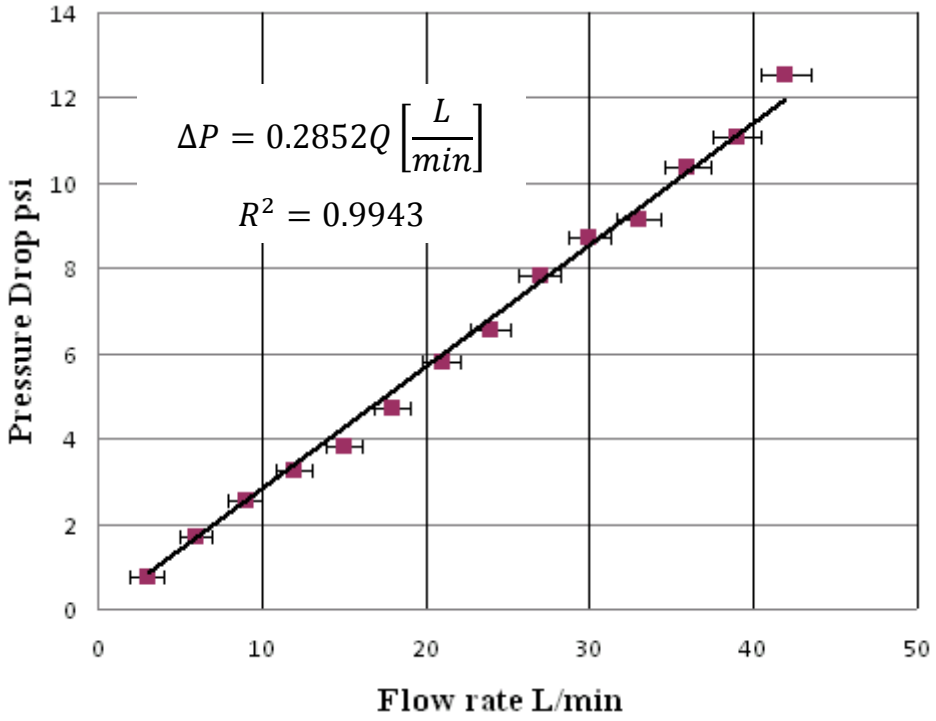

Figure 4.2.1: ΔP vs. Volume Flow Rate Through Unsifted Activated Powdered Carbon

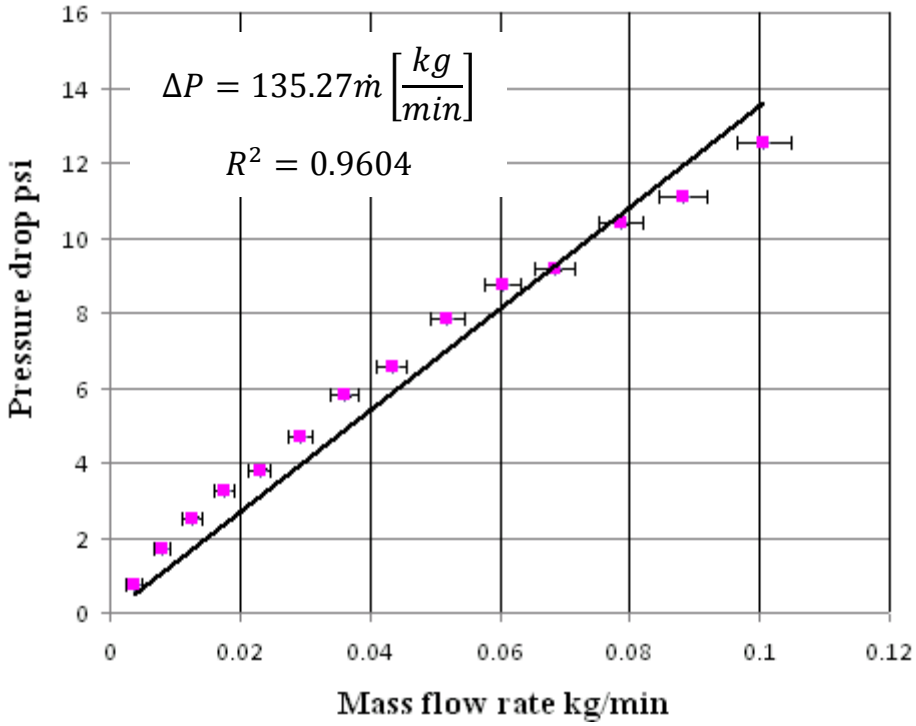

Figure 4.2.2: ΔP vs. Mass Flow Rate Through Unsifted Activated Powdered Carbon

In both Figures 4.2.1 and 4.2.2 a linear fit was made, with the equation and R^2 values displayed on the graph. Figure 4.2.3 is the plot of the compressible Darcy's law used to find the permeability.

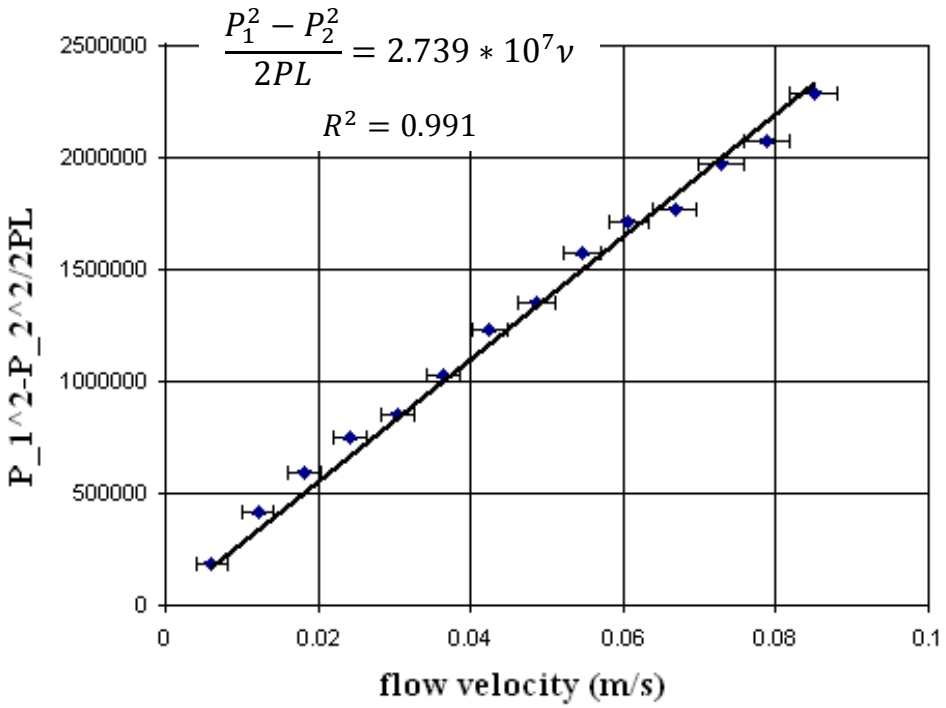

Figure 4.3.2: Plot of compressible Darcy's law used to find permeability for unsifted powder

With a value of $1.78*10^{-5}$kg/m·s for nitrogen's dynamic viscosity, μ, it was determined that the permeability, K, was $6.5*10^{-13}$ m^2.

Table 4.2.1 gives the physical properties of the unsifted powder that was used in the pressure drop experiment. Information is included for sifted powder for comparison.

Table 4.2.1: Physical Properties of Carbon in Pressure Drop Experiment.

	Density (kg/m^3)	Porosity	Cross Sectional Area (m^2)	Thickness of Powder (m)
Unsifted	415.0 ±0.3 (0.07%)	0.8122±0.00014 (0.17%)	$0.008225 \pm 1.55 * 10^{-6}$ (0.02%)	$0.02642 \pm 1.27 * 10^{-5}$ (0.005%)
Sifted	498.8 ±0.3 (0.07%)	0.7743±0.00015 (0.20%)	$0.008225 \pm 1.55 * 10^{-6}$ (0.02%)	$0.02642 \pm 1.27 * 10^{-5}$ (0.005%)

For the pressure drop experiment sifting increased the density by 20.198% and decreased the porosity by 4.670%. The difference in densities from the thermal to pressure drop experiments must be due to the qualitative nature of determining when the sample volume was full. The heights of the samples differed, for the pressure drop the depth of the powder was approximately 1 inch while in the thermal experiments it was 2.3 and 5.8 inches for the sifted and unsifted runs, respectively. This does not seem to cause the powder to be denser simply from the weight of the powder above it. While the data for these individual porosities is valid, it is difficult to control the porosity for a given mixture of particle size using an agitation and gravity method of compaction.

5.0 Discussion

5.1 Comparison of measured thermal conductivities to literature

To verify the results of the measured thermal conductivity for the powdered activated carbon a literature study was conducted and compiled in Table 5.1.1

Table 5.1.1: Thermal Conductivity Measurements for Activated Carbon From Literature

Type of Activated Carbon	Particle size (mm)	Density (kg/m^3)	Porosity	Thermal Conductivity (W/m·K)	Reference
Granular	—	460	0.781	0.11	[36]
Granular	1.04-2.6	620	0.705	0.19	[37]
Granular	2.0 (average)	500	0.762	0.3055	[38]
Granular	0.653-1.585	360	0.829	0.017	[39]
Theoretical	—	609	0.71	0.431	[40]
Theoretical Powder	0.006	480	0.771	0.105-0.21	[41]
Consolidated (with $CaCl_2$)	—	600	0.7143	0.3 (k_{teflon}=0.2 W/m·K)	[36]
PTFE binded pellet bricks	—	250	0.881	0.12 (k_{teflon}=0.2 W/m·K)	[42]
PTFE binded pellet bricks	—	400	0.810	0.11 (k_{teflon}=0.2 W/m·K)	[42]
PTFE binded pellet bricks	—	435	0.793	0.17	[42]
Monolithic (granular precursor)	—	600	0.714	0.33	[43]
Monolithic (granular precursor)	—	750	0.643	0.44	[43]
Monolithic (granular precursor)	—	840	0.600	0.7	[43]
Solidified Granular with pitch binder	0.653-1.585	600	0.714	0.305	[39]
Powder	—	235	0.888	0.15	[44]
Powder	—	269	0.892	0.27	[44]

Looking at Table 5.1.1 it is clear that a wide range of thermal conductivities were found in previous studies. While most granular carbons had poor thermal conductivity, one [38] had a much higher thermal conductivity than others. Granular samples have a much more tortuous path for the heat to follow than other samples due to the large particle size which result in larger voids. The powders also had low thermal conductivity [44], but their densities were also much lower than those used in this study. When comparing the thermal conductivity of the activated carbon powder to that of the monolithic and solidified carbons it is important to note that they are an effective thermal conductivity and that the binder can affect the conductivity of the sample. Cacciola et al.[42] concluded that PTFE(Teflon) had a large effect, since a singular solid grain had a thermal conductivity of 1.06W/m·K, much higher than the conglomerate's effective thermal conductivity. Monolithic carbon [44], while having densities up to 840 kg/m^3 is infused with an organic binder to hold it in its compact form [18]. This organic binder affects the overall thermal conductivity of the monolithic carbon. Many organic binders [45] [46] [47] are made of cellulose, which has a thermal conductivity of approximately 0.040-0.044 W/m·K[48], thus lowering the overall effective thermal conductivity of the monolithic carbon body. The monolithic carbons were able to achieve the highest thermal conductivities in spite of cellulose's low thermal conductivity due to their high densities. All previous studies of bound activated carbon samples with densities around 600kg/m^3 had thermal conductivities that were similar, most being less than 6% from the average, 3.11 W/m·K. The results for the thermal conductivity of the current samples of powdered activated carbon were higher than expected, surpassing all previous samples with similar densities. This is discussed further in section 5.2.

5.2 Effects of density on thermal conductivity of sample

Particle size had a large effect on the properties of the powder bed. When comparing the unsifted sample to the sample where all the particles were smaller than 40μm there is a 65% increase in density while only losing 11% of the powder's porosity. The difference is much smaller for the samples from the permeability experiment, with only an increase of 20% in the density and a reduction of 4.7% in porosity. This means that finer powders would be able

to adsorb more per unit volume than the coarse ones. In addition, the thermal conductivity was increased 36% by simply removing particles with diameters larger than 40μm. When comparing the current samples of powders to those used previously [44], the densities were 18.4% and 28.7% lower than the unsifted powder's. This resulted in conductivities that were 38.6% and 65.9% less than the unsifted powder's. While this seems like a large increase the previously measured powders [44] had a 44.4% increase in thermal conductivity but only a 12.6% increase in density.

5.3 Effects of PVC thermal conductivity on measured carbon thermal conductivity

The thermal conductivity of the PVC pipe that contained the powdered carbon during the thermal experiment was estimated from Tseng et al.[22] based upon the density of the foam core PVC pipe. Large uncertainty in this value could have an impact on the measured thermal conductivity of the powder. Looking at Eqn. 2.3.4 we see that the thermal conductivity of the powder is shifted by a value proportional to the thermal conductivity of the PVC. The chosen value of k_{pvc} is a reasonable one but the uncertainty in its value was estimated to be ±3%. Table 5.3.1 shows the values of k_{pdr} for k_{pvc} ±3% and ±10%.

Table 5.3.1: Effects of kpvc of kpdr

	k_{pvc}	k_{pdr} unsifted	k_{pdr} sifted
+ 3%	0.16814	0.4356	0.5925
- 3%	0.15834	0.4385	0.5953
+10%	0.17956	0.4324	0.5892
-10%	0.14691	0.4417	0.5986

Looking at Table 5.3.1 it is possible to see that the influence with just a ±3% change in k_{pvc} is not significant due to the large A_{pdr} to A_{pvc} ratio and even a ±10% error in the estimation of k_{pvc} still has k_{pdr} within the limits of uncertainty specified in Table 4.1.1.

5.4 Pressure Drop and Permeability

The high resistance to flow causes the flow to be laminar as indicated by the linear trend in the pressure drop as shown in Figures 4.2.1 and 4.2.2. Unfortunately the pressure drop through the sifted powder could not be obtained due to an accident where the powder was ejected from the pressure apparatus. The increase in the density of the sifted powder would cause the pressure drop to have been higher, resulting in a steeper slope of ΔP versus volume and mass flows and a lower permeability. The value obtained for the permeability of the sample, $6.5*10^{-13}$ m^2, is greater, by about 18 times, than those seen for dense monolithic carbons [17]. The lack of a binder resulted in a higher permeability even though the densities were similar. While the permeability is lower than the 10^{-12} required for a low pressure AC system[12], such as a carbon-methanol system, it is high enough that mass transfer limitations should not be a problem in a high pressure system such as carbon-ammonia.

5.5 Future work: Adsorber design

Now that the thermal conductivity and permeability of the activated carbon powder is known work can be done to optimize the design of an adsorber in a carbon-ammonia refrigeration system. The author proposes using a shell and tube design similar to that shown in Figure 5.5.1.

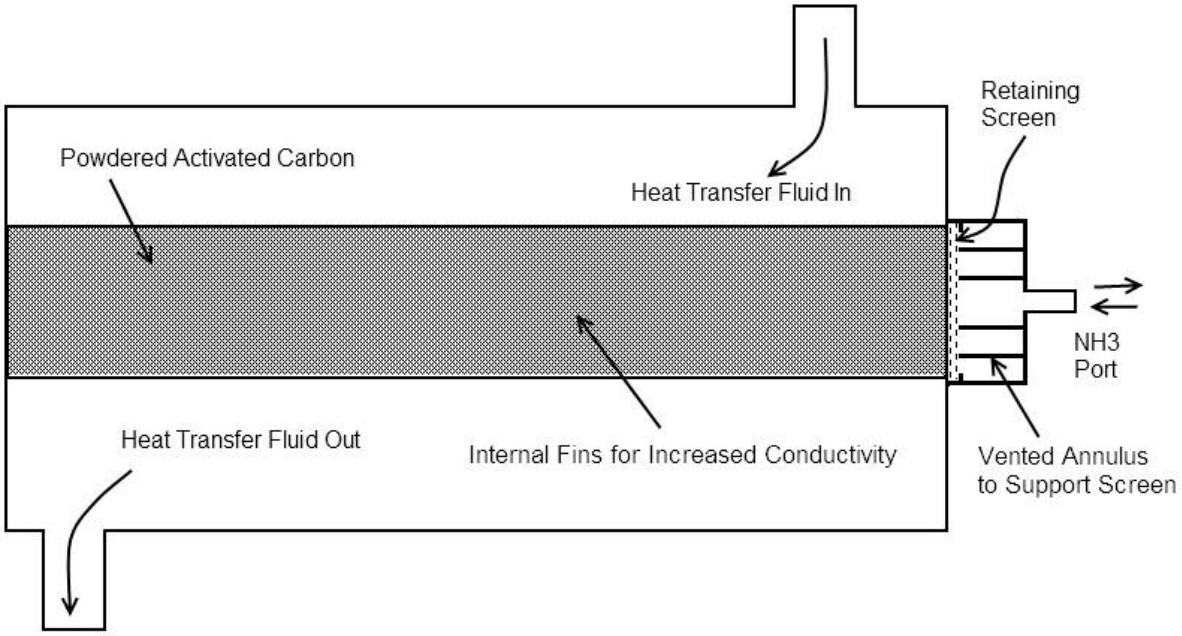

Figure 5.5.1: Proposed Adsorber design

This design is simple but allows for the implementation of internal fins and particle retention while being able to withstand the high pressures of the carbon-ammonia system. Also gas flow channels are not necessary since activated carbon- ammonia is a high pressure system and it can be assumed that the resistance to mass transfer is negligible [49]. The heat transfer fluid path does not have to withstand high pressures and provides good surface area contact to the carbon container.

5.5.1 Important design aspects

Important aspects to consider when designing the adsorber are: ammonia is corrosive so stainless steel must be used; a retention screen must be used to isolate the adsorbate; a carbon-ammonia system runs at high pressure, approximately 3MPa (435 psi); and reductions in non-adsorbate mass improve system performance. It is unfortunate that ammonia is corrosive to aluminum and copper as heat transfer is important for improving performance of the system, but stainless steel is approximately 30 times more thermally conductive than the

carbon (k≈15 W/m·K) with other mild steels being even more conductive (k ≈54 W/m·K) [24]. Stainless steel should be used for all aspects of the system that are in contact with the ammonia and water to prevent corrosion. Other more conductive steels may be used where only ammonia is present, such as the internal fins and containment tube. The retention screen is an important aspect of an adsober design that utilizes a powdered adsorber, as escaped particles can foul control valves or the expansion valve. This screen must also be constrained in a manner that keeps particles from escaping and provides support since such a fine screen must be used. The author proposes using concentric cylinders with ventilation holes. These cylinders are represented in Figure 5.5.1 by the horizontal lines to the right of the retaining screen. Lastly, a reduction in non-adsorbate mass results in a more efficient system as less material has to be heated and cooled during the refrigeration cycle.

5.5.2 Adsorption limits

The ammonia adsorption limits of the tested powdered activated carbon should be tested and matched to a concentration equation such as the Dubin-Radushkevich [17] equation shown Eqn. 5.5.1

$$x = x_0 \left[-\kappa \left(\frac{T}{T_{sat}} - 1 \right)^n \right] \qquad \text{Eqn. 5.5.1}$$

where x is the concentration of ammonia in the carbon (kg NH_3/kg carbon), x_0 is the maximum ammonia concentration under saturation conditions, T is the carbon temperature in Kelvin, T_{sat} is the saturation temperature, κ and n are constants found by experimental results. This is necessary to estimate the amount of ammonia that is adsorbed at the operating temperatures of the system. While many different carbons have been tested for the adsorption limit of ammonia, [14] the values can vary significantly even for the same type of carbon bed(granular, powder, monolithic etc). With the adsorption limit known it is possible to calculate the required volume of the adsorbate. The process for this calculation is explained in [13]. A calculation in [13], assuming the adsorption system is replacing a 5.0kW compressor system, requires 0.696 kg of ammonia to be desorbed during the heating phase of

the adsorber. The mass of adsorbate required is then estimated based upon the adsorption limits of the adsorbate. With the knowledge of the density of the activated powdered carbon it is then possible to know what volume of carbon is required for the desired system output. One should note that a denser carbon body takes less space to hold the same amount of ammonia, but usually cannot adsorb as much ammonia per unit mass of carbon as the porosity is lower. A balance must be found that gives the smallest required volume. One additional positive side effect of a smaller volume is less material to heat and cool, increasing performance of the system.

5.5.3 Optimization of the Adsorber

Areas that need to be optimized are: Diameter and thickness of activated carbon container; thickness and number of fins to enhance heat transfer in carbon; and fin type (pin, radial, steel wool). To properly optimize the adsorber a computer routine that models incorporating both heat and mass transfer in the adsorbate should be used such as by Sun et al. [49], Al Mers et al. [50] or Corral [51]. This model would predict system COP as a function of one of the variables to be optimized and in this manner the design of the adsorber can be optimized. While mass transfer is not a limiting factor in high pressure systems, if the adsorber is required to be long, say greater than 0.5m, than an assessment of the effects of length should be explored as well. To increase permeability a gas channel would have to be added using a fine retention screen, adding to the complexity of the adsorber.

6.0 Conclusions

Powdered activated carbon is a prime candidate for use in an adsorption refrigeration cycle, with a thermal conductivity just as high as some variants of monolithic carbon and an ability to adsorb more ammonia.

Other methods of sifting the powder should be explored, as a gravity based method would be too slow for commercial viability. One solution might be to use a compressed gas coupled with agitation to force the particle through the screens instead of using gravity to do this.

Deceases in particle size will increase the thermal conductivity and density of the powder bed, but at the expense of porosity and permeability of the bed. Additional studies could be done to further study the effects of sample particle size on porosity. An apparatus that pressed a known mass of carbon powder to a predetermined volume might accomplish this. However, activated carbon when fully compacted has a high density, 2210 kg/m^3, but this is undesirable as the porosity is zero and no adsorption would be possible.

Another challenge in working with powdered activated carbon is that it is very difficult to contain. Very small particles go through even 325 x 2300 mesh screens, which could lead to fouling of a refrigeration system. The use of finer screens to eliminate this is possible, but such fine screens are very expensive, and restrict flow.

With the information gained from these experiments further work must be done to optimize the design of an adsorber. The only remaining experimental work to be done before simulations is a characterization of ammonia absorbance, and then simulations to optimize the adsorber could follow.

Knowing the thermal conductivity of powdered activated carbon is a necessary component to design efficient adsorber banks for an operational unit. This work shows that powdered activated carbon should be considered for a solid adsorption refrigeration cycle to cool a passenger compartment utilizing otherwise wasted heat energy in the exhaust of the engine. This work has significance as the focus on energy efficiency, especially in passenger

vehicles, increases. Reductions in accessory loads such as the AC, is a viable option to reach fuel efficiency goals.

REFERENCES

1. National Highway Traffic Safety Administration, http://www.nhtsa.gov/fuel-economy, Washington, DC [downloaded 5 July 2010].

2. **Gado, A., Hwang, Y.,** and **Radermacher, R.** Dynamic Behavior of Mobile Air-Conditioning Systems. *HVAC&R Research,* 2008, **Vol. 14**, **No. 2**, 307-321

3. **Lambert, M. A.** and **Jones, B. J.** Automotive adsorption air conditioner powered by exhaust heat. Part 1: conceptual and embodiment design. *Proc, IMechE Part D: J. Automobile Engineering,* 2006, **Vol. 220**, 959-972

4. **Thacher, E. F., Helenbrook, B. T., Karri, M. A.,** and **Richter, C. J.** Testing of an automobile exhaust thermoelectric generator in a light truck. *Proc, IMechE Part D: J. Automobile Engineering,* 2007, **Vol. 221**, 95-107

5. **Boatto, P., Boccaletti, C., Cerri, G.,** and **Malvicino, C.** Internal combustion engine waste heat potential for an automotive absorption system of air conditioning Part 2: the automotive absorption system. *Proc, IMechE Part D: J. Automobile Engineering,* 2000, **Vol. 214**, 983-989

6. **Koehler, J., Tegethoff, W. J., Westphalen, D., Sonnekalb, M.** Absorption refrigeration system for mobile applications utilizing exhaust gases, *Heat and Mass Transfer,* 1997 ,**Vol. 32**, 333-340

7. **Meunier, F.** Solid sorption heat powered cycles for cooling and heat pumping applications, *Applied thermal Engineering,* 1998, **Vol. 18**, 715-729

8. **Qu, T. F., Wang, W.,** and **Wang, R. Z.** Study of the Effects of Mass and Heat Recovery on the Performances of Activated Carbon/Ammonia Adsorption Refrigeration Cycles, *Journal of Solar Energy Engineering,* 2002, **Vol. 124**, 283-290

9. **Wang, R.,** and **Wang, L.** Adsorption refrigeration cooling driven by low grade thermal energy, *Chinese Science Bulletin,* 2005, **Vol. 50**, **No. 3**, 193-204

10. **Critoph, R. E.** Evaluation of Alternative Refrigerant-Adsorbent Pairs for Refrigeration Cycles, *Applied Thermal Engineering*, 1996, **Vol. 16**, **No. 11**, 891-900

11. **Lee, S.,** and **Bae, C.** The application of an exhaust heat exchanger to protect the catalyst and improve the fuel economy in a spark-ignition engine, *Proc, IMechE Part D: J. Automobile Engineering*, 2007, **Vol. 221**, 621-628

12. **Critoph, R. E.,** and **Zhong, Y.** Review of trends in solid sorption refrigeration and heat pumping technology, *Proc, IMechE Part E: Process Mechanical Engineering*, 2005, **Vol. 219**, 285-300

13. **Lambert, M. A.** and **Jones, B. J.** Automotive adsorption air conditioner powered by exhaust heat. Part 2: detailed design and analysis. *Proc, IMechE Part D: J. Automobile Engineering*, 2006, **Vol. 220**, 973-989

14. **Tamainot-Telto, Z., Metcalf, R.E., Critoph, R. E., Zhong, Y.,** and **Thorpe, R.** Carbon-Ammonia pairs for adsorption refrigeration applications: ice making, air conditioning and heat pumping, *International Journal of Refrigeration*, 2009, **Vol. 32**, 1212-1229

15. **Chahbani, M. H., Labidi, J.,** and, **Paris, J.** Modeling of adsorption heat pumps with heat regeneration, *Applied Thermal Engineering*, 2004, **Vol. 24**, 431-447

16. **Tamainot-Telto, Z., Metcalf, R.E.,** and **Critoph, R. E.** Novel compact sorption generators for car air conditioning, *International Journal of Refrigeration*, 2009, **Vol. 32**, 727-733

17. **Tamainot-Telto, Z.,** and **Critoph, R. E.** Thermophysical properties of monolithic carbon, *International Journal of Heat and Mass Transfer*, 2000, **Vol. 43**, 2053-2058

18. **Critoph, R. E., Tamainot-Telto, Z.,** and **Davies, G. N. L.** A prototype of a fast cycle adsorption refrigerator utilizing a novel carbon-aluminum laminate, *Proc, IMechE Part D: J. Automobile Engineering*, 2000, **Vol. 214**, 439-448

19. Screen Technology Group, Inc. http://www.wovenwire.com/dutch-twilled-weave.htm, Washougal, WA, updated 15, March 2009

20. MeadWestvaco Corporation. http://www.meadwestvaco.com/SpecialtyChemicals/ActivatedCarbon/MWV003519 Covington, VA, Revised April 2009

21. Tseng, A. A., Borrosky, M. A., O'Conner, S. M., and **Knotts, J. J.** Impact Behavior of Modified PVC for Outdoor Applications, *Advances in Polymer Technology*, 1991, **Vol. 10**, **No. 3**, 205-218

22. Wark, K. Jr. *Thermodynamics*, Ed. 5, 1988, New York: McGraw-Hill

23. Chen, X., and **Penumadu, D.,** Permeability Measurement and Numerical Modeling for Refractory Porous Materials, American Foundry Society Transactions, 2008, **Vol. 116**, Paper 08-133(11), 1045-1059

24. Holman, J. P., *Heat Transfer*, Ed. 7, 1990, New York: McGraw-Hill

25. Kline, S. J., and F. A. McClintock. Describing Uncertainties in Single-Sample Experiments. *Mechanical Engineering*, 1953, **Vol. 75**, **No. 1**, 3-8

26. Omega Engineering Inc. Revised Type T Thermocouple Reference Tables, www.omega.com, Stamford, CT

27. Omega Engineering Inc. OMB-DAQ-56 product manual, www.omega.com, Stamford, CT

28. Omega Engineering Inc. PX01-C1 spec sheet, www.omega.com, Stamford, CT

29. Fluke Corporation, "8060 A" Digital multimeter users manual, https://us.fluke.com, Everett, WA

30. Mettler-Toledo, PM4800 DeltaRange digital scale, Applications, Technical Data, Accessories, http://us.mt.com/us/en/home.html, Columbus, OH

31. Jaytech Glass Ltd, Class B spout cylinders, http://jaytecglass.co.uk/index.php East Sussex, UK

32. TELEDYNE Technologies Inc., Hastings 203 series instructions manual, http://www.teledyne.com/, Thousand Oaks, CA

33. Noranzyk, A, Thermal Conductivity Measurements of Graphite Samples, Required work for internship at Los Alamos National Laboratory, 2009

34. Holman, J. P., *Experimental Methods for Engineers*, Ed. 7, 2001, New York: McGraw-Hill

35. Budaiwi, I., Abdou,. A., and **Al-Homoud, M.** Variations of Thermal Conductivity of Insulation Materials Under Different Operating Temperatures: Impact on Envelope-Induced Cooling Load, *Journal of Architectural Engineering*, 2002, **Vol. 8**, **No. 4**, 125-132

36. Wang., L. W., Wang, R. Z., Lu, Z. S., Chen, C. J., Wang, K., and **Wu, J. Y.** The performance of two adsorption ice making test units using activated carbon and a carbon composite as adsorbents, *Carbon*, 2006, **Vol. 44**, 2671-2680

37. Wu, J. Y., Tang, Z. M., Shi, W., and **Wang, R. Z.** Research on Measuring Method of the Thermal Conductivity for Highly Porous Materials, *ACTA Metallurgica Sinca*, 1997, **Vol. 10**, **No. 3**, 213-218

38. Aghbalou, F., Mimet, A., Badia, F., Illa, J., El Bouardi, A., and **Bougard, J.** Heat and mass transfer during adsorption of ammonia in a cylindrical adsorbent bed: thermal performance study of a combined parabolic solar collector, water hat pipe and adsorber generator assembly, *Applied Thermal Engineering*, 2004, **Vol. 24**, 2537-2555

39. **Wang, L. W., Wu, J. Y., Wang, R. Z., Xu, Y. X., Wang, S. G.,** and **Li, X. R.** Study of the performance of activated carbon-methanol adsorption systems concerning heat and mass transfer, *Applied Thermal Engineering*, 2003, **Vol. 23**, 1605-1617

40. **El Fadar, A., Mimet, A., Azzabakh, A., Pérez-García, M.,** and **Castaing, J.** Study of a new solar adsorption refrigerator powered by a parabolic trough collector, *Applied Thermal Engineering*, 2009, **Vol. 29**, 1267-1270

41. **Basumatary, R., Dutta, P., Prasad, M.,** and **Srinivasan, K.** Thermal modeling of activated carbon based adsorptive natural gas storage system, *Carbon*, 2005, **Vol. 43**, 541-549

42. **Cacciola, G., Restuccia, G.** and **Mercandante, L.** Composites of Activated Carbon for Refrigeration Adsorption Machines, *Carbon*, 1995, **Vol. 33**, **No. 9**, 1205-1210

43. **Tamainot-Telto, Z.,** and **Critoph, R. E.** Advanced solid sorption air conditioning modules using monolithic carbon-ammonia pair, *Applied Thermal Engineering*, 2003, **Vol. 23**, 659-674

44. **Jones, J. C.** Indirect evidence of relatively high thermal conductivities in powdered activated carbons, *Fuel*, 1998, **Vol. 77**, **No. 14**,

45. **Robinson, K. K., Mieville, R. L.** *Monolithic Activated Carbon*, US Patent No. 6,207,264 B1, March 27, 2001

46. **Bookbinder, D. C., DeLiso, E. M., Johnson, R. E.,** and **Streicher, K. P.** *Activated Carbon Bodies Having Phenolic Resin Binder*, US Patent No. 5,379,325, February 14, 1995

47. **McCrae, P. D. A., Zhang, T.,** and **Walker, D. R. B.** *Shaped Activated Carbon*, US Patent No. 6,472,343 B1, October 29, 2002

48. Kehrer, M., Künzel, H. M., and **Sedlbauer, K.** *Ecological Insulation Materials – Does Sorption Moisture Affect their Insulation Performance?*, Journal of Thermal Envelope and Building Science, 2003, **Vol. 26**, **No. 3**, 207-212

49. Sun, L. M., Ben Amar, N., and **Meunier, F.** Numerical Study on Coupled Heat and Mass Transfers in an Adsorber With External Fluid Heating, *Heat Recovery Systems & CHP*, 1995, **Vol. 15**, **No. 1**, 19-29

50. Al Mers, A., Azzabakh, A., Mimet, A., and **El Kalkha, H.** Optimal design study of cylindrical finned reactor for solar adsorption cooling machine working with activated carbon-ammonia pair, *Applied Thermal Engineering*, 2006, **Vol. 26**, 1866-1875

51. Corral, F. Enhancement of Heat Transfer in an Adsorbent Bed, Master's Thesis San Jose State University, 2001